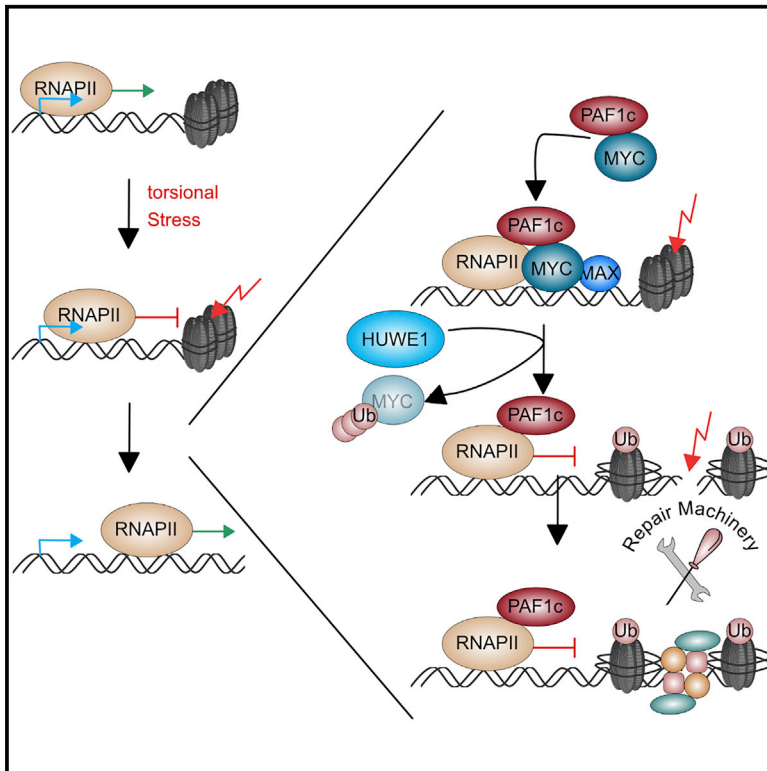


Ubiquitylation of MYC couples transcription elongation with double-strand break repair at active promoters

Graphical Abstract



Authors

Theresa Endres, Daniel Solvie,
Jan B. Heidelberger, ..., Elmar Wolf,
Peter Gallant, Martin Eilers

Correspondence

martin.eilers@
biozentrum.uni-wuerzburg.de

In Brief

Endres et al. demonstrate that the E3 ligase HUWE1 drives the transfer of the elongation complex PAF1c from MYC onto the RNA polymerase II. This transfer promotes the repair of double-strand breaks to maintain genome integrity in MYC-driven tumors.

Highlights

- MYC and PAF1c interact directly and bind promoters interdependently
- PAF1c is rapidly transferred from MYC onto RNAPII
- The transfer is driven by HUWE1 and is required for MYC-dependent transcription
- MYC and HUWE1 promote histone H2B ubiquitylation
- MYC suppresses double-strand break accumulation in a PAF1c-dependent manner



Article

Ubiquitylation of MYC couples transcription elongation with double-strand break repair at active promoters

Theresa Endres,^{1,9} Daniel Solvie,^{1,9} Jan B. Heidelberger,² Valentina Andrioletti,³ Apoorva Baluapuri,⁴ Carsten P. Ade,¹ Matthias Muhar,⁵ Ursula Eilers,⁶ Seychelle M. Vos,^{7,8} Patrick Cramer,⁷ Johannes Zuber,⁵ Petra Beli,² Nikita Popov,³ Elmar Wolf,⁴ Peter Gallant,¹ and Martin Eilers^{1,10,*}

¹Theodor Boveri Institute, Department of Biochemistry and Molecular Biology, Biocenter, University of Würzburg, 97074 Würzburg, Germany

²Institute of Molecular Biology (IMB), Ackermannweg 4, 55128 Mainz, Germany

³Internal Medicine VIII—Clinical Tumor Biology, University of Tübingen, Otfried-Müller-Straße 14, 72076 Tübingen, Germany

⁴Cancer Systems Biology Group, Department of Biochemistry and Molecular Biology, Biocenter, University of Würzburg, 97074 Würzburg, Germany

⁵Research Institute of Molecular Pathology, Campus Vienna Biocenter 1, 1030 Vienna, Austria

⁶Core Unit High-Content Microscopy, Biocenter, University of Würzburg, 97074 Würzburg, Germany

⁷Department of Molecular Biology, Max Planck Institute for Biophysical Chemistry, Am Fassberg 11, 37077 Göttingen, Germany

⁸Massachusetts Institute of Technology, Department of Biology, 31 Ames Street, Cambridge, MA 02139, USA

⁹These authors contributed equally

¹⁰Lead contact

*Correspondence: martin.eilers@biozentrum.uni-wuerzburg.de

<https://doi.org/10.1016/j.molcel.2020.12.035>

SUMMARY

The MYC oncoprotein globally affects the function of RNA polymerase II (RNAPII). The ability of MYC to promote transcription elongation depends on its ubiquitylation. Here, we show that MYC and PAF1c (polymerase II-associated factor 1 complex) interact directly and mutually enhance each other's association with active promoters. PAF1c is rapidly transferred from MYC onto RNAPII. This transfer is driven by the HUWE1 ubiquitin ligase and is required for MYC-dependent transcription elongation. MYC and HUWE1 promote histone H2B ubiquitylation, which alters chromatin structure both for transcription elongation and double-strand break repair. Consistently, MYC suppresses double-strand break accumulation in active genes in a strictly PAF1c-dependent manner. Depletion of PAF1c causes transcription-dependent accumulation of double-strand breaks, despite widespread repair-associated DNA synthesis. Our data show that the transfer of PAF1c from MYC onto RNAPII efficiently couples transcription elongation with double-strand break repair to maintain the genomic integrity of MYC-driven tumor cells.

INTRODUCTION

Deregulated expression of the MYC oncoprotein or one of its paralogs, MYCN and MYCL, drives tumorigenesis in many entities (Dang, 2012). Tumors driven by a number of different oncogenes continuously depend on enhanced MYC expression, suggesting that targeting MYC is a valid approach for tumor therapy (Anni-bali et al., 2014; Beaulieu et al., 2019; Gabay et al., 2014; Soucek et al., 2013). MYC proteins are transcription factors that bind to virtually all active promoters and many active enhancers (Kress et al., 2015). While MYC generally stimulates the transcription by RNA polymerases I (RNAPI) and III, its effects on the expression of individual genes transcribed by RNAPII can be both positive and negative (Herold et al., 2019; Sabò et al., 2014; Tesi et al., 2019; Walz et al., 2014). In addition, MYC-dependent global increases in the expression of all mRNAs have been

observed (Lin et al., 2012; Nie et al., 2012). Both the general and specific effects of MYC on gene expression are typically weak, raising the possibility that MYC proteins have functions that are independent of altering target gene expression (Baluapuri et al., 2020).

The stepwise assembly of an elongation-competent RNAPII complex is a well-understood process (Cramer, 2019). MYC proteins affect several steps of this process, and their ability to promote transcription elongation is predominant in numerous experiments (Baluapuri et al., 2019; de Pretis et al., 2017; Herold et al., 2019; Rahl et al., 2010; Walz et al., 2014). Several lines of evidence show that MYC engages not only CDK9 (Huang et al., 2014; Rahl et al., 2010) but also the ubiquitin system to promote transcription elongation. First, several MYC-associated ubiquitin ligases are required for MYC-driven gene expression (Adhikary et al., 2005; Kim et al., 2003; von der Lehr et al., 2003). Inhibitors



of the HUWE1 ubiquitin ligase abrogate MYC-dependent gene expression in colorectal tumor cells (Peter et al., 2014). Conversely, the dephosphorylation of MYCN enables binding of USP11, which leads to transcription termination (Herold et al., 2019). Second, a lysine-free mutant of MYC is capable of recruiting RNAPII to core promoters but fails to promote pause release (Jaenicke et al., 2016). Finally, transcriptional activation by MYC requires ubiquitin-dependent extraction of MYC from chromatin by the p97/VCP complex (Heidelberger et al., 2018).

Ubiquitylation of MYC is required for the transfer of the PAF1c transcription elongation complex from MYC onto RNAPII (Jaenicke et al., 2016). Since MYC-dependent transcriptional elongation also depends on CDK9, our previous data did not distinguish between 2 possible models: the first model suggests that the actual transfer of PAF1c from MYC onto RNAPII is driven by CDK9, with ubiquitylation of MYC removing non-productive protein complexes from promoters. The other model suggests that the transfer itself is driven by the ubiquitylation of MYC. To address the question of how the ubiquitin system promotes MYC-dependent transcriptional elongation, we have analyzed the mechanism of transferring PAF1c from MYC onto RNAPII and the consequences of disrupting this process.

RESULTS

PAF1c binds MYC directly and enhances the association of MYC with active promoters

The inhibition of proteasome function in HeLa cells strongly enhances the binding of MYC to CTR9 and CDC73, 2 subunits of the PAF1 complex (PAF1c) (Jaenicke et al., 2016). To test whether this association reflects a direct interaction of MYC with this complex, we incubated a purified glutathione-S-transferase (GST)-MYC fusion protein that encompasses amino acids 1–163 of human MYC with purified PAF1c, which has been reconstituted from recombinantly expressed subunits (Vos et al., 2018a) (Figures 1A and 1B); note that the PAF1c used lacks the RTF1 subunit (Vos et al., 2018a). PAF1c was recovered on beads carrying GST-MYC, but not on beads with an equivalent amount of GST (Figure 1C). Amino acids 1–163 of MYC encompass a large part of the transcription regulatory domain and include the highly conserved MYCBoxes I and II (Balupuri et al., 2020). Neither MYCBox I nor MYCBox II were required for interaction with PAF1c, which is consistent with recent Bio-ID data for 2 PAF1c subunits, CDC73 and PAF1 (Figure 1D) (Kalkat et al., 2018).

On chromatin, MYC binds preferentially to active promoters and this preference depends on protein-protein interactions of MYC with promoter-bound factors (Guo et al., 2014; Lorenzin et al., 2016). To determine whether PAF1c is required for the specific binding of MYC to active promoters, we stably expressed short hairpin RNAs (shRNAs) targeting 2 subunits of PAF1c, CTR9 and CDC73, in U2OS cells using lentiviral infection. Since the vector used for depletion confers resistance to puromycin, infected cells were selected and used 96 h after infection without further passaging. Each shRNA depleted its target protein by ~80% (Figures 1E and S1A). To precisely evaluate possible changes in chromatin association, we used spike-in chromatin immunoprecipitation sequencing (ChIP-seq; ChIP with reference exogenous genome [ChIP-Rx]) (Orlando et al., 2014). Depletion

of CTR9 or CDC73 caused a 2- to 3-fold decrease in the association of MYC with active promoters (Figures 1F and S1B). Subsequent analyses also showed that the decrease in MYC binding upon CTR9 or CDC73 depletion occurred at promoters but not at enhancers (Figure S1C), which is consistent with previous observations for *Drosophila* Myc (Gerlach et al., 2017).

Stable depletion of CTR9 or CDC73 also caused a reduction of ~30% in total MYC protein levels, most likely due to a reduction in MYC mRNA levels (Figures 1E and S1A). To rule out the possibility that this decrease accounted for the apparent decrease in MYC binding, we expressed doxycycline (Dox)-inducible shRNAs targeting CTR9 or CDC73 in cells stably expressing ectopic MYC. With ~80,000 molecules of MYC per cell, U2OS cells express relatively low endogenous MYC levels, and stable lentiviral expression raises the number to $\sim 1 \times 10^6$ molecules per cell (Lorenzin et al., 2016). In cells expressing ectopic MYC, the addition of Dox led to a 3-fold reduction in the levels of the respective target protein, but had no effect on MYC levels (Figures S1D–S1F). Density plots and browser tracks confirmed that the depletion of CTR9 and, to a lesser degree, of CDC73 reduced the binding of MYC to promoters, while it had little or no effect on MYC binding to enhancers (Figures 1G and S1G–S1I). We concluded that MYC binds directly to PAF1c and that PAF1c is required for the preferential association of MYC with active promoters.

Rapid transfer of PAF1c from MYC onto RNAPII

PAF1c travels with elongating RNAPII (Van Oss et al., 2017). To determine whether MYC affects the loading of PAF1c onto RNAPII, we analyzed the binding of RNAPII to chromatin by ChIP-seq of unperturbed U2OS cells and compared it to cells in which MYC was stably expressed from a lentiviral promoter. Metagene plots showed that ectopic expression of MYC had little effect on the chromatin association of total RNAPII, but strongly enhanced the levels of elongating Ser2-phosphorylated RNAPII (pS2 RNAPII) downstream of the start site and in the gene body, consistent with multiple previous data that MYC promotes elongation (Rahl et al., 2010; Walz et al., 2014) (Figure 2A). In parallel, the ectopic expression of MYC strongly enhanced the association of both CTR9 and CDC73 with chromatin in gene bodies, and the depletion of either protein using specific shRNA confirmed the specificity of the ChIP signal (Figures 2B, S2A, and S2B). Stratifying the response for MYC occupancy at the promoter showed that the increase in the association of pS2, CTR9, and CDC73 with gene bodies was much stronger on genes with strongly MYC-bound (“top”) than on weakly MYC-bound (“bottom”) promoters (Figures 2A and 2B). Importantly, while the depletion of CTR9 had no obvious effect on the distribution of total RNAPII, it reverted the MYC-dependent increase in pS2 association with chromatin in promoter-proximal regions, gene bodies, and transcription end site regions, demonstrating that the transfer of PAF1c is required for MYC-driven transcription elongation (Figures 2A and 2B).

To test how quickly PAF1c is transferred from MYC onto RNAPII, we used U2OS cells that carry a hormone-inducible MYCER chimeric protein and harvested cells 10 and 30 min after the addition of 200 nM 4-OHT. The activation of MYC had no effect on the total levels of CTR9, CDC73, RNAPII, or pS2 RNAPII

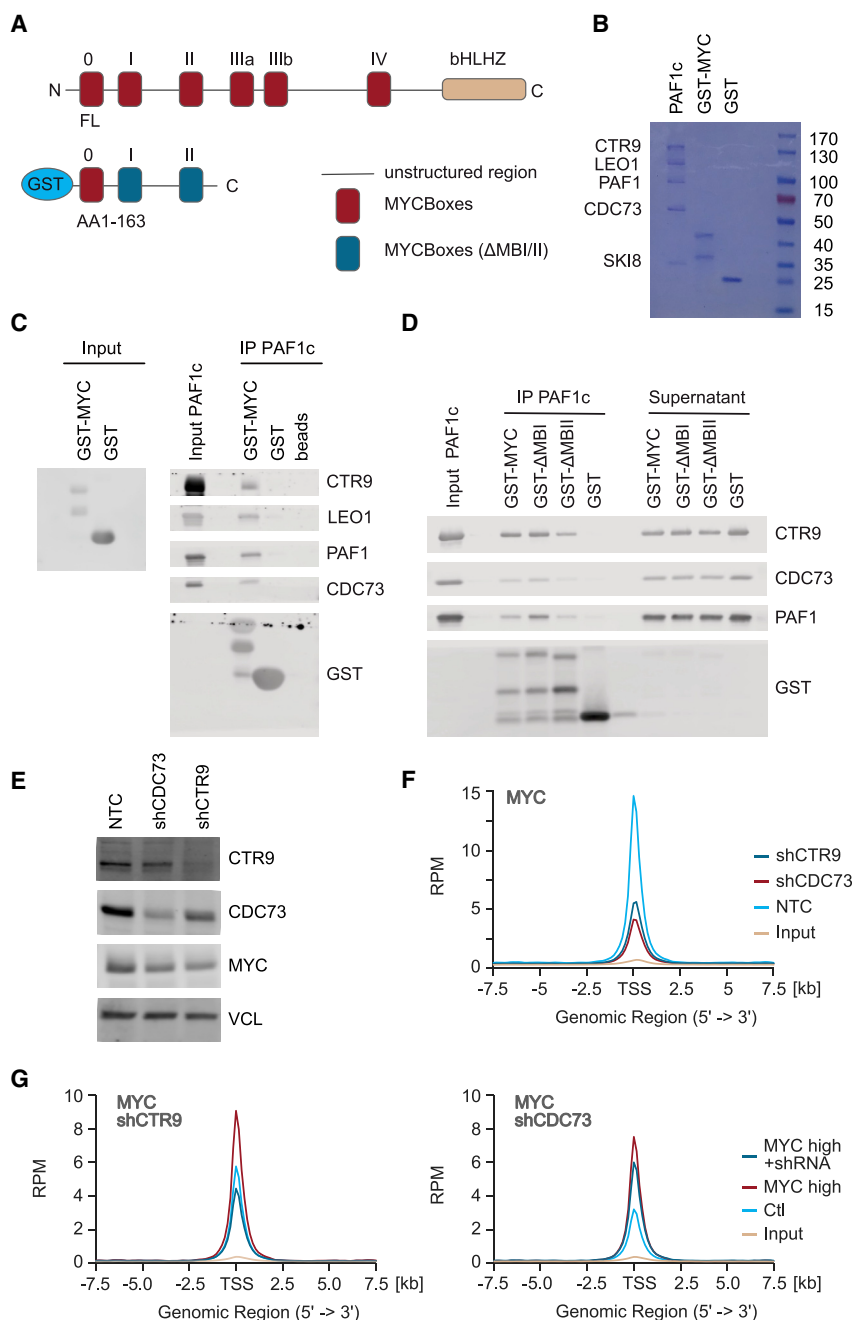


Figure 1. Binding of PAF1c to MYC enhances association of MYC with active promoters

(A) Diagram of MYC protein structure showing the position of MYCBoxes and the GST-MYC construct used for pull-down experiments.

(B) Coomassie gel showing purified proteins; 10% of input material is shown.

(C) Immunoblots of MYC and PAF1c (n = 3; in all legends, n indicates the number of independent biological replicates).

(D) Immunoblots of pull-down experiment using GST-ΔMYCBox I and GST-ΔMYCBox II constructs (n = 3).

(E) Immunoblot showing levels of CTR9, CDC73, and MYC in U2OS cells after stable expression of constitutive shRNAs. Vinculin (VCL) was used as loading control (n = 3).

(F) Density plot of MYC centered on the transcription start site (TSS) of 8,437 active promoters in a ChIP-Rx experiment in control U2OS cells or in cells expressing shCTR9 or shCDC73 (n = 1). All ChIP-seq traces show SEM as a shade.

(G) Density plot of MYC as in (F) in a ChIP experiment in control U2OS cells or in cells stably expressing MYC and Dox-inducible shRNA targeting CTR9 (shCTR9) or shCDC73 (n = 1). See also Figure S1.

at these short time points (Figure 2C). ChIP-Rx experiments revealed a strong increase in MYC association with promoters (Figure S2C) and an increase in the association of pS2 RNAPII with chromatin in gene bodies downstream of the transcription start site (TSS) at 10 min after MYC activation (Figures 2D and S2D), and a further increase at 30 min. These data are consistent with previous data showing that MYC promotes the pause release of RNAPII (Rahl et al., 2010; Walz et al., 2014). We did not detect an increase in the association of PAF1c with gene bodies 10 min after MYC activation, but did detect a strong increase at 30 min, demonstrating that MYC-dependent PAF1c

association with chromatin in promoter or gene body regions (Figure 2F, right panel). As before, the extent of the decrease in CDC73 correlated with MYC occupancy of the promoter (Figure 2F). We concluded that MYC recruits PAF1c to active promoters and that PAF1c is rapidly transferred from MYC onto RNAPII following MYC-dependent pause release.

HUWE1 drives the transfer of PAF1c from MYC onto RNAPII

We next used proximity ligation assays (PLAs) with PAF1 and MYC antibodies to understand how PAF1c is transferred from

transfer is delayed relative to pause release (Figures 2D and S2D).

Conversely, we wanted to know whether the high levels of MYC found in human tumor cells are rate limiting for the association of PAF1c with RNAPII. Since U2OS cells express relative low levels of endogenous MYC, we used K562 cells, the endogenous MYC of which has been replaced by a chimeric protein, in which MYC is fused to an auxin-induced degron (AID) (Muhar et al., 2018). In these cells, the addition of indole-3 acetic acid (IAA) induces rapid degradation of the MYC-AID chimera (Figures 2E and S2E). Importantly, the addition of IAA for 30 min led to a significant decrease in the association of CDC73 with gene bodies (Figure 2F, left panel). At this early time point, this decrease was not secondary to a decrease in RNAPII as-

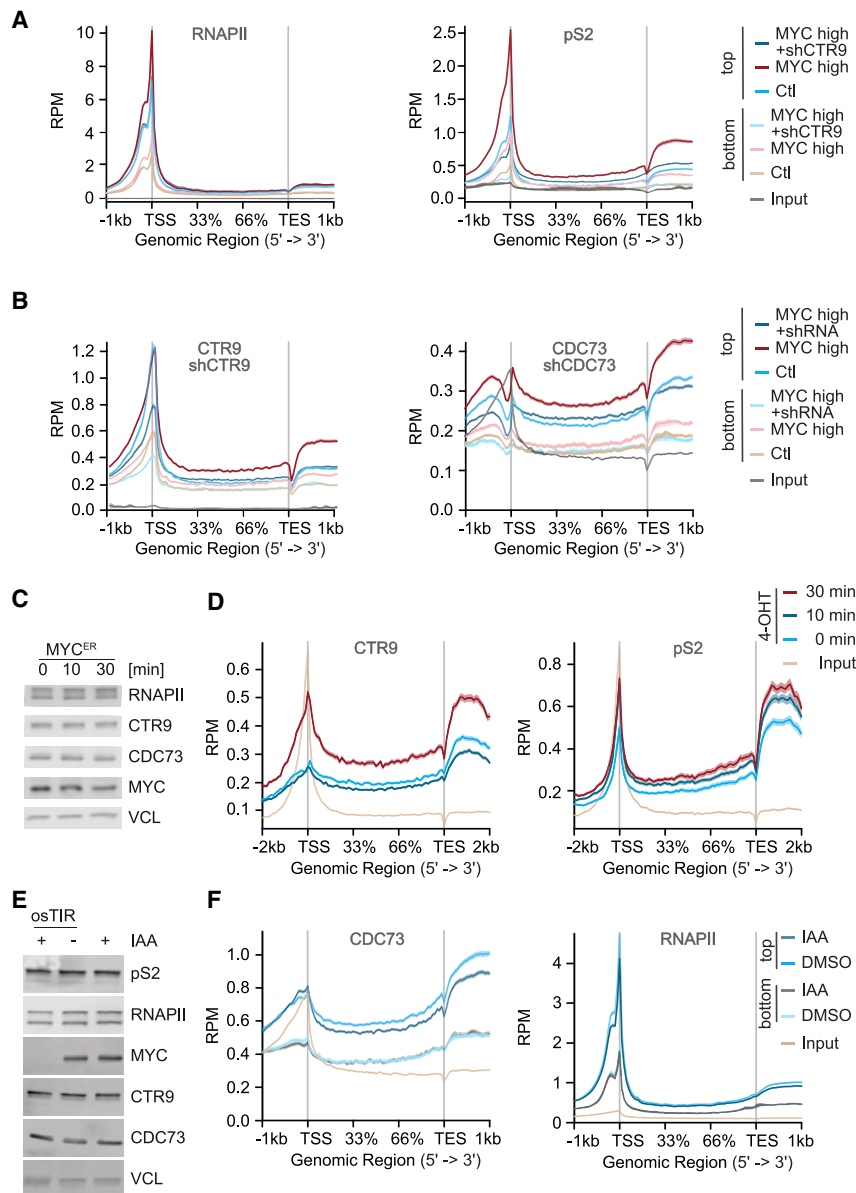


Figure 2. PAF1c is rapidly transferred from MYC on RNAPII

(A) Metagenes plot of total RNAPII or pS2 RNAPII in a ChIP experiment in control U2OS cells or in cells stably expressing MYC and Dox-inducible shCTR9; metagenes plots of 7,479 most strongly MYC-bound (“top”) or 5,768 weakly MYC-bound (“bottom”) genes are shown (see STAR methods). Input shows 17,697 genes. Chromatin of 6 independent experiments was pooled for ChIP-seq.

(B) Metagenes plot of CTR9 or CDC73 binding to chromatin in a ChIP experiment, in control U2OS cells, or in cells stably expressing MYC and Dox-inducible shCTR9 or shCDC73; metagenes plots of top or bottom MYC-bound genes. Input shows 17,697 genes. Chromatin of 6 independent experiments was pooled for ChIP-seq.

(C) Immunoblot of U2OS cells expressing a MYCER chimeric protein with or without MYC activation upon addition of 4-OHT (200 nM) for 10 or 30 min.

(D) Metagenes plot of CTR9 and pS2 in a ChIP-Rx experiment in U2OS MYCER cells treated as described in (C). The plot shows profiles of the top 4,000 MYC-bound genes (n = 2).

(E) Immunoblot of K562-MYC-AID erythroleukemia cells (n = 2). Indole-3-acetic acid (IAA; 100 μM) was added for 30 min. VCL was used as loading control (n = 3).

(F) Metagenes plot of CDC73 or total RNAPII in a ChIP-Rx experiment in K562-MYC-AID cells treated as in (E). Metagenes plots of top or bottom MYC-bound genes (n = 2). Input shows 17,697 genes.

See also Figure S2.

MYC onto RNAPII. Controls established that the signal obtained with PAF1c and MYC antibodies was specific, since it did not occur when only one antibody was added and was dependent on Dox-inducible induction of MYC (Figure 3A). Consistent with our previous experiments, inhibition of the proteasome by MG132 strongly enhanced the PLA signal between MYC and PAF1 (Figure 3A) (Jaenicke et al., 2016). In contrast, inhibition of CDK9 using a specific inhibitor, NVP-2 (Olson et al., 2018), decreased the PLA signal between MYC and PAF1 (Figure 3A). This is consistent with observations that CDK9 phosphorylates the C-terminal domain (CTD) of RNAPII and the negative elongation factor (NELF) complex and causes it to dissociate from RNAPII (Fujinaga et al., 2004). The dissociation of NELF frees the interaction surface for PAF1c on RNAPII (Vos et al., 2018a, 2018b), arguing that

the inhibition of CDK9 precludes PAF1c from interacting with MYC at core promoters.

To better understand the dependency of PAF1c transfer on the ubiquitin system, we screened small interfering RNAs (siRNAs) targeting all ubiquitin ligases that have been reported in the literature to associate with MYC or MYCN using the proximity of MYC with the PAF1c subunit PAF1 as readout (Figures 3B and S3A). The depletion

of several ligases significantly enhanced the proximity of MYC with PAF1 in cells. To focus on core promoters, we performed a second screen using the proximity of PAF1 with Ser5-phosphorylated (pS5) RNAPII, which is strongly enriched at core promoters (Figure S3B). This showed that the siRNA-mediated depletion of three ubiquitin ligases significantly enhanced the extent of the association of PAF1c with RNAPII (Figure S3B). The overlap of both screens identified the ubiquitin ligase HUWE1 as a significant hit of both screens (Figures 3C and 3D). HUWE1 has been shown to bind to MYC and be required for transcriptional activation by MYC (Adhikary et al., 2005; Baluapuri et al., 2019; Peter et al., 2014).

To rapidly perturb HUWE1 function and study its impact on MYC and RNAPII function, we used a previously characterized inhibitor of HUWE1, BI8626 (Peter et al., 2014). This inhibitor

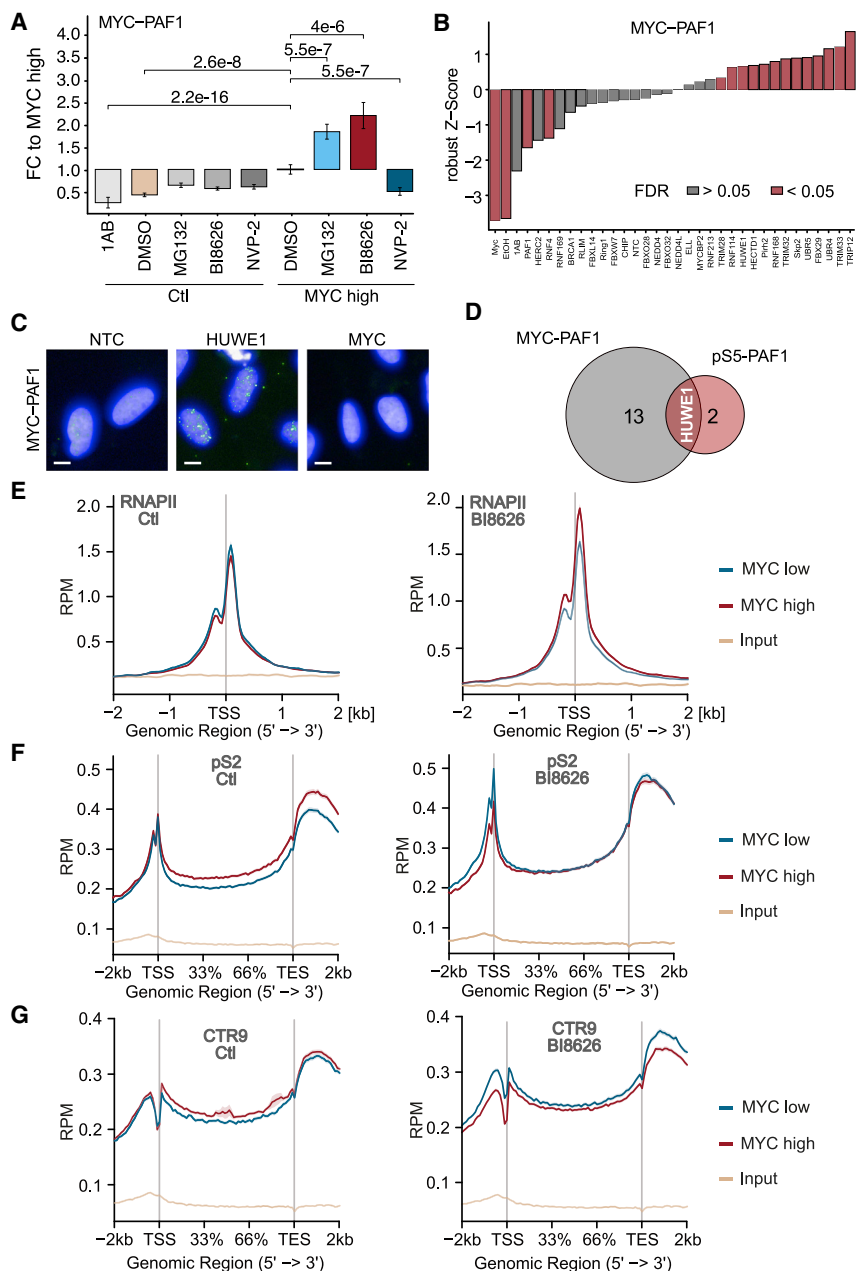


Figure 3. The HUWE1 ubiquitin ligase drives the transfer of PAF1c from MYC onto RNAPII

(A) Boxplot of proximity ligation assays (PLAs) between MYC and PAF1 in U2OS cells expressing Dox-inducible MYC. Where indicated (“MYC high”), Dox (1 μ g/mL) was added for 24 h, MG132 (20 μ M), BI8626 (10 μ M), and NVP2 (1 μ M) was added for 4 h (n = 3). 1AB refers to control samples containing solely the anti-PAF1 antibody. Statistical significance was calculated using Wilcoxon rank sum test. (B) Results of a siRNA screen targeting MYC-associated ubiquitin ligases using PLAs between MYC and PAF1 as readout (n = 10).

(C) Representative micrographs. Nuclei were stained with Hoechst; bright dots indicate the proximity of MYC with PAF1. Scale bar: 10 μ m.

(D) Venn diagram of siRNAs significantly enhancing the proximity between the corresponding proteins.

(E) Metagene plot of total RNAPII in a ChIP-Rx experiment in U2OS cells expressing Dox-inducible MYC. The plots show metagene profiles of all active promoters (n = 17,674) with or without the addition of Dox in control (DMSO-treated) cells or cells exposed to BI8626 (n = 2).

(F) Metagene plot of pS2 RNAPII in a ChIP-Rx experiment. Plots and conditions are as in (E) (n = 2).

(G) Metagene plot of CTR9 in a ChIP-Rx experiment. Plots and conditions are as in (E) (n = 2).

See also Figure S3.

(Figure S3C, left), and very few changes in ubiquitylation at individual sites differed between inhibitor and siRNA (Figure S3C, right). A notable exception was HUWE1 itself, since multiple ubiquitylation sites on HUWE1 decreased in abundance upon depletion but not upon the inhibition of HUWE1, suggesting that the corresponding ubiquitylation sites are targeted by other ligases (Figure S3C, right). We concluded that the HUWE1 inhibitor targets a spectrum of ubiquitylation sites that are largely direct or indirect targets of HUWE1.

While the impact of HUWE1 depletion on the steady-state levels of soluble MYC is weak, ubiquitylation by HUWE1 extracts MYC from chromatin via the p97 ATPase

blocks the activity of HUWE1, but not that of other HECT (homologous to the E6-AP carboxyl terminus)-domain ubiquitin ligases, and blocks MYC-dependent transcriptional activation in colorectal cancer cells. We confirmed that BI8626 enhances the MYC/PAF1-PLA signal to a similar degree as the depletion of HUWE1 (Figure 3A). To better characterize its mode of action in cells and to ascertain the specificity of BI8626, we performed ubiquitin remnant profiling (Kim et al., 2011; Xu et al., 2010) in U2OS cells, in which we depleted HUWE1 using a siRNA, and compared this to inhibitor-treated cells. We were able to identify a total of 1,825 ubiquitylated sites across 4 individual experiments. The changes in ubiquitylation in response to the depletion of HUWE1 highly correlated with those of HUWE1 inhibition

(Heidelberger et al., 2018). Consistent with this, incubation of U2OS cells with BI8626 or the VCP inhibitor NMS-873 (Magnaghi et al., 2013) enhanced MYC occupancy at the *Nucleolin* (NCL) promoter (Figure S3D), while neither depletion nor inhibition of HUWE1 affected the levels of soluble MYC (Figure S3E). To globally test the effects of HUWE1 inhibition on MYC levels and on RNAPII function, we performed ChIP-Rx-seq from U2OS cells that carry Dox-inducible MYC at physiological levels of MYC or after induction of MYC by the addition of Dox for 24 h. Metagene plots of all expressed genes showed that the inhibition of HUWE1 caused a small increase in MYC association at promoters at the physiological MYC level and a much larger increase in cells expressing ectopic MYC (Figure S3F). The

induction of ectopic MYC expression in control cells had no obvious effect on the chromatin association of total RNAPII, but it did cause a significant accumulation of RNAPII close to the transcription start site when HUWE1 was inhibited (Figure 3E). Consistent with multiple previous data, the induction of MYC caused a large increase in pS2 RNAPII within the gene body and the transcription end site in control cells (Figure 3F). The inhibition of HUWE1 abrogated the MYC-dependent increase in elongation. Instead, the induction of MYC caused a small decrease in the association of pS2 RNAPII with promoter-proximal regions in the presence of BI8626 (Figure 3F). Finally, the induction of MYC increased the association of CTR9 with gene bodies in control cells, but it decreased the association of CTR9 with chromatin in the gene body upon HUWE1 inhibition (Figure 3G). We concluded that blockade of HUWE1 abolishes the ability of MYC to promote transcription elongation and exposes an ability of MYC to retain RNAPII close to the promoter. Notably, the phenotype is similar to that observed in response to the expression of a lysine-free mutant of MYC, supporting the notion that a decrease in the ubiquitylation of MYC itself is critical for the effects of HUWE1 inhibition (Jaenicke et al., 2016).

MYC and HUWE1 promote global histone H2B ubiquitylation

We performed two experiments to confirm that MYC and HUWE1 do not act upstream of NELF to promote the transfer of PAF1c onto RNAPII. First, immunoblots did not reveal a global HUWE1-dependent change in the phosphorylation of RNAPII at serines 2 and 5 (Figure 4A). Second, we generated NELF ChIP-seq data and used them to show that MYC promotes transcription elongation and promotes the transfer of CTR9 both on genes with NELF-bound promoters and on genes that do not have NELF bound at their promoters (Figures S4A and S4B). We concluded that HUWE1 does not promote RNAPII pause release via CDK9 and NELF. Since PAF1c does not bind to RNAPII when NELF is bound, we suggest that MYC together with HUWE1 stimulates elongation from promoters after the CDK9-dependent dissociation of NELF. This interpretation is consistent with observations that NELF acts upstream of the actual release of RNAPII into the gene body (Aoi et al., 2020).

RTF1, a subunit of PAF1c, interacts directly with and activates the BRE1A/B (RNF20/40) ubiquitin ligase, which mono-ubiquitylates histone H2B at K120 (Kim et al., 2009; Van Oss et al., 2016), suggesting that HUWE1 and MYC act upstream of histone H2B ubiquitylation to modulate RNAPII function. To test this hypothesis, we precipitated lysates of U2OS cells expressing Dox-inducible MYC before and after incubation with a HUWE1 inhibitor with an anti-ubiquitin antibody. Under these conditions, the induction of MYC increased the ubiquitylation of histone H2B and this was suppressed by the inhibition or siRNA-mediated depletion of HUWE1 (Figures 4B and S4C). ChIP-Rx-seq confirmed that histone H2B ubiquitylation at expressed genes is globally suppressed upon HUWE1 inhibition, while total levels of H2B remain unaffected (Figures 4C and S4D). HUWE1-dependent ubiquitylation of MYC was detectable on paused but not on non-paused genes (Figure S5A) and occurred both on NELF-bound and non-NELF-bound genes (Figure S5B), supporting

the view that the ubiquitylation of MYC contributes to MYC-dependent pause release and occurs independent of the CDK9-dependent NELF release from RNAPII (Aoi et al., 2020; Jaenicke et al., 2016). To confirm that these effects reflect an on-target activity of HUWE1 inhibitors, we generated an HCT116 cell line, which carries a bi-allelic knockin replacing the cysteine residue of HUWE1 that forms a thioester with ubiquitin with a serine (Figure 4D). Both immunofluorescence (Figure 4E) and immunoblots of cell lysates (Figure 4F) showed a significant decrease in histone H2B ubiquitylation. We concluded that HUWE1 and MYC globally control H2B ubiquitylation at active genes.

MYC promotes double-strand repair in transcribed regions

Ubiquitylation of histone H2B supports both transcriptional elongation (Fuchs et al., 2014) and the opening of chromatin for the repair of double-strand breaks (Moyal et al., 2011; Nakamura et al., 2011). Transcription-dependent breaks occur due to torsional stress that can be relieved by the recruitment of topoisomerases; inhibition of topoisomerase II, therefore, induces double-strand breaks both in gene bodies and, most strongly, downstream of active promoters (Gothe et al., 2019; Kouzine et al., 2013; Singh et al., 2020). To test whether MYC enhances DNA repair, we blocked topoisomerase II using a specific inhibitor, etoposide, and asked whether the induction of MYC suppresses the formation of double-strand breaks using BLISS sequencing (breaks labeling *in situ* and sequencing) (Yan et al., 2017).

Consistent with previously published observations (Madabhushi et al., 2015), a limited number of double-strand breaks were detectable downstream of the TSS of actively transcribed genes, but not at weakly expressed genes (Figure 5A). The addition of etoposide strongly increased the number of promoter-proximal breaks on active genes. The induction of MYC by Dox had only a small effect on the number of breaks in control cells, but it did suppress the accumulation of etoposide-induced double-strand breaks at active promoters and gene bodies. Conversely, the depletion of MYC in K562-AID cells enhanced the accumulation of breaks after etoposide treatment at active promoters; notably, the depletion of MYC in the absence of etoposide actually decreased double-strand frequency, most likely due to a decreased overall transcription rate (Figure S5C). The depletion of CTR9 caused a strong increase in double-strand breaks around the TSS and in gene bodies of actively transcribed, but not of weakly expressed, genes, and the addition of etoposide did not lead to a further increase in double-strand break accumulation (Figure 5B). Importantly, the induction of MYC was unable to revert the shCTR9-dependent increase in double-strand breaks (Figure 5B).

The effects of MYC and etoposide were strongest at highly expressed genes (Figure 5A), and neither MYC nor etoposide caused significant changes in double-strand breaks in heterochromatin (Figure S5D). While the total number of breaks per promoter correlated with overall gene expression, MYC reverted the etoposide-induced increase in breaks on both highly and weakly expressed genes, on genes that showed pausing of RNAPII and on non-paused genes, and on both MYC-activated

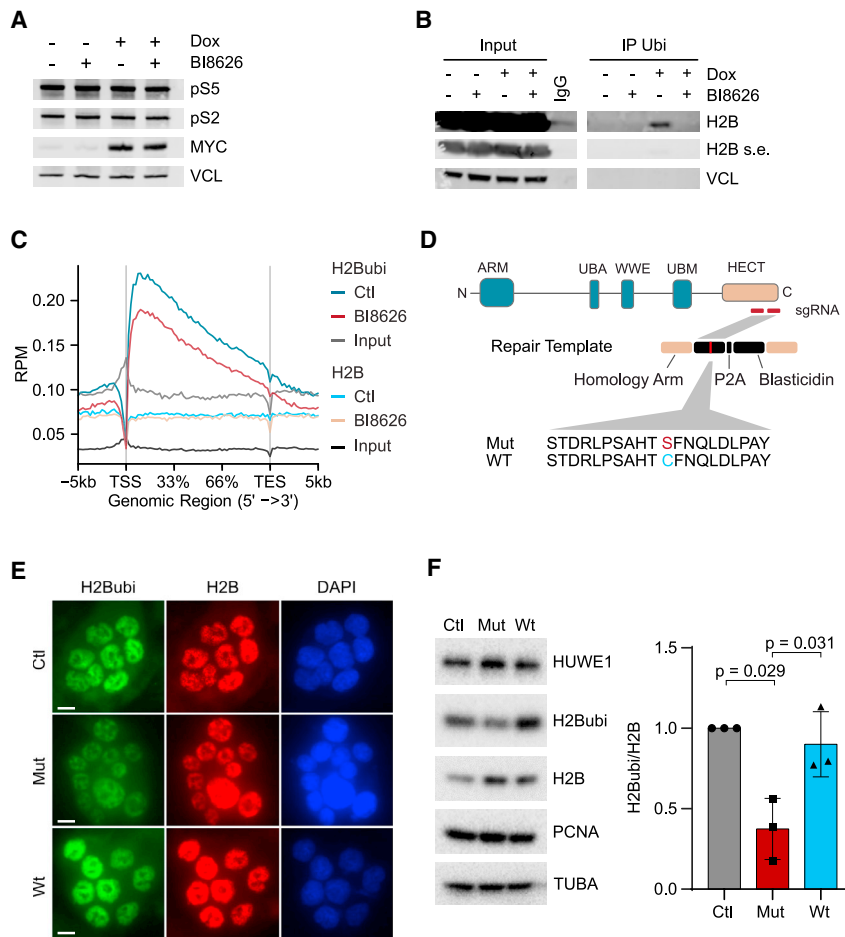


Figure 4. HUWE1 and MYC control global histone H2B ubiquitylation

(A) Immunoblot of U2OS cells with or without induction of MYC in the presence or absence of BI8626 (n = 2).

(B) Immunoprecipitation using an anti-ubiquitin antibody (FK2) from U2OS cells. Input shows 1% of the material used in the immunoprecipitation (n = 2). A shorter exposure (s.e.) was chosen to visualize total H2B levels.

(C) Metagene plot of a ChIP-Rx experiment of ubiquitylated H2B (“H2Bubi”) and H2B in U2OS cells expressing Dox-inducible MYC after the addition of DMSO-treated cells or cells exposed to BI8626. The metagene plot shows the profile of all of the active promoters (n = 2).

(D) Diagram illustrating knockin mutagenesis strategy toward the catalytic cysteine of HUWE1.

(E) Immunofluorescence of H2Bubi levels in wild-type HCT116 cells (“Ctl”) and in cells upon bi-allelic replacement of the catalytic cysteine of HUWE1 with serine (“Mut”). As control, HCT116 cells, in which a repair template with cysteine (“Wt”) was used, are shown (n = 3). Scale bar: 10 μm.

(F) Left: Immunoblot (see Figure 5D for description) (n = 3). Right: quantification of the results. Tubulin (TUBA) was used as loading control. Data show means ± SDs (n = 3). Statistical significance was calculated using Welch’s t test. See also Figure S4.

expression of 2 different shRNAs each and found that depletion of either protein retarded the proliferation of U2OS cells with or without the induction of MYC (Figures 6A and S6A). RNA-seq confirmed that MYC exerted both weakly positive

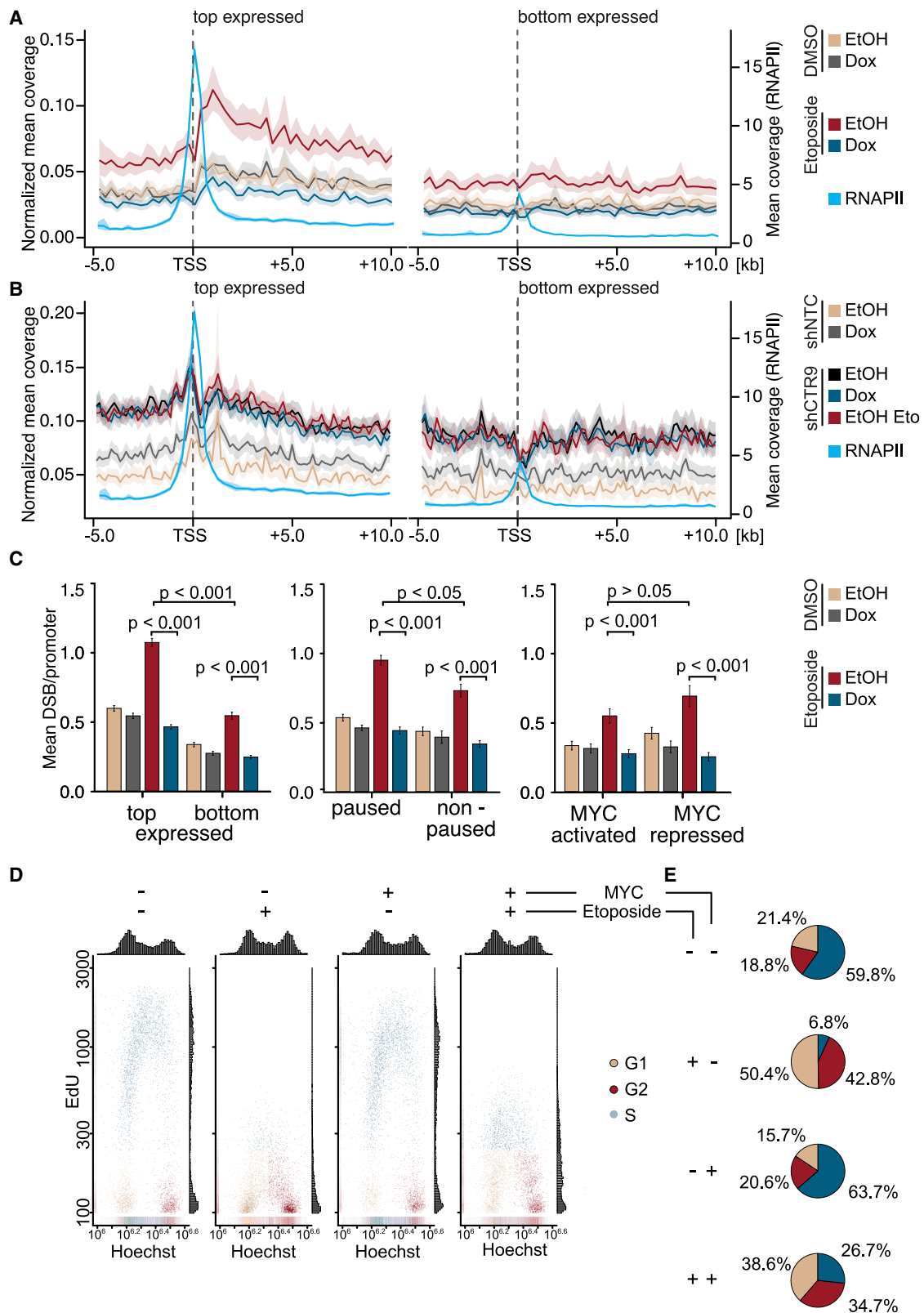
and MYC-repressed genes, arguing that the effects of MYC on the accumulation of double-strand breaks are independent of the effects on gene expression (Figure 5C). MYC also reverted the etoposide-induced increase uniformly when promoters were stratified by the number of breaks (Figure S5E). To test whether MYC has an effect on cellular responses to etoposide, we performed cell-cycle analyses of U2OS cells that were exposed to etoposide for 3 h both with and without the induction of MYC. Consistent with multiple previous data, etoposide strongly suppressed the DNA synthesis in control cells (Figure 5D). While the induction of MYC had only a small effect on the cell-cycle distribution of U2OS cells in the absence of etoposide (Walz et al., 2014), it restored DNA synthesis in etoposide-treated cells to a significant degree (Figures 5D and 5E). While the experiment does not distinguish between replicative DNA synthesis and DNA synthesis associated with DNA repair, the data show that MYC promotes the repair of promoter-proximal DNA breaks and alleviates the inhibition of DNA synthesis in response to topoisomerase inhibition.

PAF1c suppresses transcription-dependent DNA damage

To assess the specific contribution of PAF1c to MYC-dependent cellular phenotypes, we depleted CTR9 or CDC73 by the stable

and negative effects on large groups of genes that have been previously described in this and multiple other systems (Figure 6B) (see Introduction). Note that the induction of MYC in the exponentially growing U2OS cells used here does not alter the total amount of mRNA per cell (Walz et al., 2014). The depletion of CTR9 or CDC73 attenuated the effects of MYC on both induced and repressed genes, consistent with the decrease in chromatin association of MYC with promoters observed in CTR9- and CDC73-depleted cells (Figure 6B).

The attenuation of MYC-dependent gene expression upon PAF1c depletion raised the expectation that depletion of either PAF1c subunit would also have mild effects on MYC-dependent cell-cycle progression. Induction of MYC activity in U2OS-MYCER cells by the addition of 4-OHT or the induction of MYC expression by Dox led to small increases in the proportion of cells in S phase of the cell cycle (Figures 6C and S6B). In contrast, the induction of MYC led to a much larger accumulation of cells in S phase of the cell cycle upon the depletion of CTR9 or CDC73, indicating a strong delay in DNA replication (Figures 6C and S6B). To understand this observation, we used antibodies that indicate activation of the ATM or the ATR kinase, reflecting double-strand breaks and replication stress, respectively (Figures 6D and S6C). While induction of MYC had little effect on the activity of these kinases under control conditions, depletion



(legend on next page)

of CTR9 or CDC73 increased the phosphorylation of H2AX and KAP1 at S824 and the additional induction of MYC led to a further increase in the phosphorylation of both proteins. Both sites are phosphorylated by the ATM kinase. In contrast, we did not observe an effect of MYC induction after CTR9 or CDC73 depletion on the phosphorylation of CHK1 (S345) or RPA S33, which are target sites of the ATR kinase, or on the phosphorylation of RPAS4/8, a target site of DNA-PK (Figures 6D and S6C). We noted that the MYC-stimulated increase in H2AX phosphorylation in CTR9-depleted cells was highest in S phase, suggesting that PAF1 complexes have a role in preventing replication-transcription conflicts (Figure 6E). The incubation of cells with specific inhibitors of CDK7 (LDC4297; Hutterer et al., 2015) or CDK9 (NVP-2; Olson et al., 2018) for 3 h strongly attenuated the induction of DNA damage in CTR9-depleted cells, demonstrating that DNA damage is caused by the residual transcription in these cells (Figures 6E and S6D).

Parallel fluorescence-activated cell sorting (FACS) analysis of propidium iodide-stained control cells, in which nascent DNA had been labeled with a pulse of bromodeoxyuridine (BrdU) revealed a normal profile with well-separated BrdU⁺ and BrdU⁻ populations (Figure S6E). Depletion of CTR9 or CDC73 led to a marked reduction in overall DNA synthesis and apparent DNA synthesis in cells with a 2n and a 4n DNA content; this phenotype was aggravated by the expression of high MYC levels (Figure S6E). The observation suggests that the DNA synthesis may be due to the repair of double-strand breaks rather than normal replication (Orthwein et al., 2015). In strong support, confocal microscopy revealed a large increase in the colocalization of γ -H2AX foci with 5-ethynyl-2'-deoxyuridine (EdU) incorporation, indicative of DNA repair-associated DNA synthesis (Figures 7A, 7B, and S7A). We concluded that PAF1c has moderate effects on MYC-dependent gene expression but coordinates elongation with DNA repair to suppress transcription-induced DNA damage (Figure 7C).

DISCUSSION

Both ubiquitylation of MYC and CDK9 are required for MYC-driven transcriptional elongation (Bywater et al., 2020; Huang et al., 2014; Jaenicke et al., 2016; Rahl et al., 2010). The CDK9-dependent dissociation of NELF frees the interaction surface for PAF1c on RNAPII (Vos et al., 2018a, 2018b), and there is a second, PAF1c-dependent pause site downstream of the NELF-dependent site (Aoi et al., 2020). Here, we showed the HUWE1-dependent ubiquitylation of MYC and transfer of PAF1c control elongation at a step downstream of the CDK9-

dependent release of RNAPII from NELF inhibition. Both in flies and in humans, binding of MYC to PAF1c at promoters has moderate effects on gene expression, raising the question of what its principal biological function may be (Gerlach et al., 2017).

Actively transcribed genes are particularly susceptible to DNA damage. To maintain genomic stability, dedicated mechanisms ensure that DNA repair is especially effective at transcribed genes (Gregersen and Svejstrup, 2018; Lans et al., 2019). The transcription process itself causes torsional stress that is a major cause for double-strand breaks in genes (Kouzine et al., 2013), and the relief of torsional stress is critical for transcription elongation (Bunch et al., 2015; Ju et al., 2006; Puc et al., 2015). Several mechanisms counteract transcription-induced torsional stress—for example, phosphorylated RNAPII stimulates the activity of topoisomerase I (Baranello et al., 2016). Also, both MYC and MYCN interact with topoisomerases I and II (Balupuri et al., 2019; Büchel et al., 2017). Nevertheless, double-strand breaks are enriched downstream of active promoters in proliferating cells (Chiarle et al., 2011; Gothe et al., 2019; Klein et al., 2011). Here, we show that MYC promotes the repair of DNA breaks via the HUWE1-dependent transfer of PAF1c from MYC to RNAPII. PAF1c in turn directly activates the BRE1A/B (RNF20/40) ligase that mono-ubiquitylates H2B (Van Oss et al., 2016). This histone modification alters chromatin structure and promotes the repair of double-strand breaks by non-homologous end joining or homologous recombination (Moyal et al., 2011; Oliveira et al., 2014). Since MYC suppresses the accumulation of double-strand breaks on genes independently of changes in steady-state mRNA levels, our observations can provide a plausible explanation for the pervasive presence of MYC proteins at virtually all active promoters (Figure 7C).

In addition to topoisomerases, 2 partner proteins of MYC and MYCN, the TRRAP-containing NuA4 complex (Jacquet et al., 2016; Kim et al., 2010; Murr et al., 2006) and the p400 helicase (Courilleau et al., 2012; Frank et al., 2003; Fuchs et al., 2001) have direct functions in double-strand break repair. Furthermore, the neuronal MYC paralog, MYCN, recruits the BRCA1 protein, a central scaffold protein of multiple complexes involved in homologous recombination (Venkitaraman, 2014), to active promoters (Herold et al., 2019). A hallmark of DNA repair proteins is that their association with RNA polymerases, replication forks, or chromatin is transient and regulated by protein ubiquitylation. Consistently, several MYC-associated ubiquitin ligases (Gudjonsson et al., 2012; Qiao et al., 2020) and MYC-associated ubiquitin-specific proteases (Herold et al., 2019; Knobel et al., 2014; Orthwein et al., 2015; Popov et al., 2007; Sondalle et al., 2019; Sun et al., 2015; Zhang et al., 2006) regulate the stability or

Figure 5. MYC promotes double-strand repair at active promoters

(A) Density plot showing normalized mean coverage and estimated confidence interval of double-strand breaks (BLISS8) and total RNAPII (ChIP-Rx) around the transcription start sites of top ($n = 3,954$; left) and bottom ($n = 3,012$; right) expressed genes in U2OS cells expressing Dox-inducible MYC. Shown is the merge of biological triplicates.
 (B) Density plot of double-strand breaks (BLISS8) and total RNAPII (ChIP-Rx) of U2OS cells expressing stable shCTR9 or non-targeting control. Shown is the merge of biological triplicates.
 (C) Stratification of double-strand breaks by promoter features. Data are means \pm SEMs. Statistical significance was calculated using Wilcoxon rank sum test.
 (D) Cell-cycle distribution and EdU incorporation in U2OS cells expressing Dox-inducible MYC. Dox and etoposide were added as described ($n = 3$); 5,000 cells are shown per condition.
 (E) Pie chart visualizing the cell-cycle distribution of U2OS treated as described in (D).
 See also Figure S5.

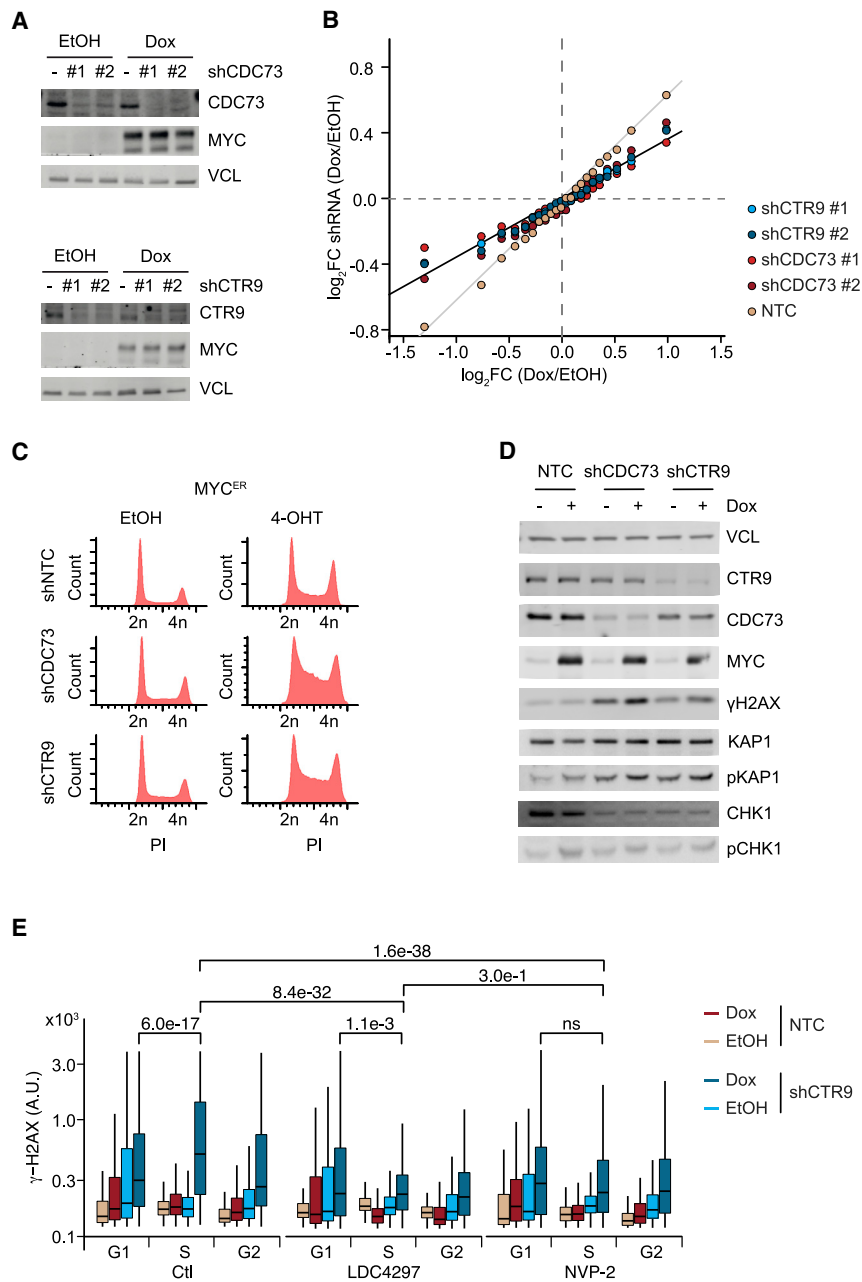


Figure 6. MYC induces rampant DNA damage in the absence of PAF1c

(A) Immunoblot of MYC in U2OS cells expressing Dox-inducible MYC and non-targeting shRNA, shCDC73 (top), or shCTR9 (bottom) (n = 4).

(B) Summary of RNA-seq experiments from the cells described in (A). Genes were sorted in 23 bins (see STAR methods). The plot shows the change in gene expression observed for each bin upon expression of the indicated shRNAs. Values are the average of 4 biological replicates using 2 different shRNAs each for CTR9 and CDC73.

(C) FACS profile of propidium-iodide stained U2OS-MYCER cells expressing shCTR9 or shCDC73 upon addition of 4-OHT (200 nM) for 24 h (n = 2).

(D) Immunoblot of U2OS cells expressing Dox-inducible MYC and non-targeting shRNA or shCDC73 or shCTR9 (n = 3).

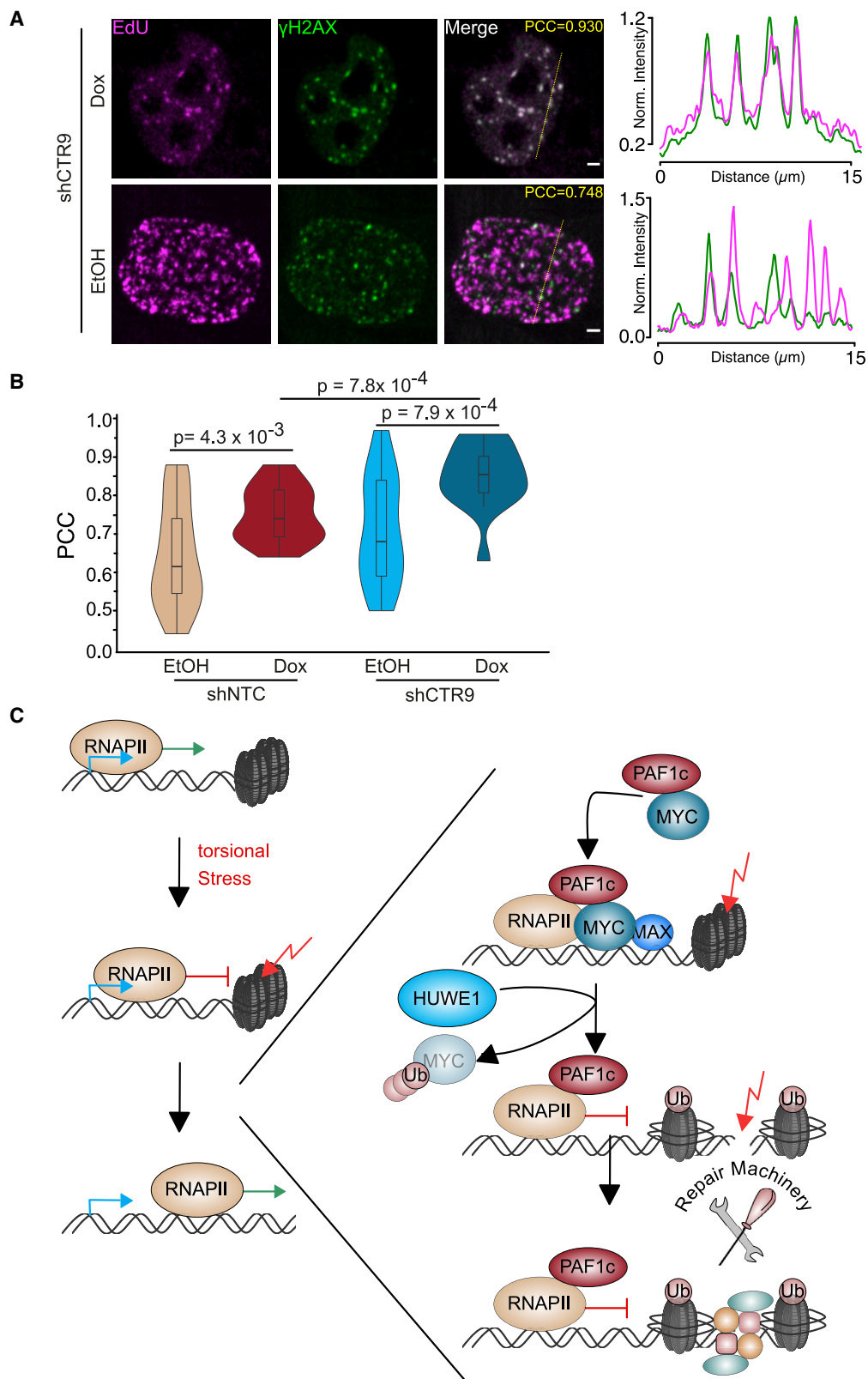
(E) Quantitative immunofluorescence of γ-H2AX in U2OS control cells (n = 3) or cells treated with the CDK7 inhibitor LDC4297 or the CDK9 inhibitor NVP-2 for 3 h. Cells were stratified for their cell-cycle position by Hoechst staining. Shown is a boxplot of the intensity of γ-H2AX for at least 800 cells. Statistical significance was calculated using Wilcoxon rank sum test.

See also Figure S6.

interactions of DNA repair proteins. We propose, therefore, that MYC proteins engage multiple complexes that suppress double-strand break accumulation at active promoters, and MYC-associated ubiquitylation and de-ubiquitylation reactions dynamically control their interactions with the transcription machinery.

Depletion of PAF1c induces transcription-dependent DNA damage, arguing that the residual transcription that occurs in depleted cells is highly DNA damaging. This increase was highest in S phase, consistent with a previous report that shows that PAF1c is critical for preventing transcription-replication conflicts (Poli et al., 2016). Such conflicts can be co-directional or head-on, with conflicts being largely head-on, since the origins of repli-

cation are localized at active promoters (Chen et al., 2019). Co-directional conflicts activate ATM but not ATR (Hamperl et al., 2017), arguing that PAF1c prevents the accumulation of breaks that occur during co-directional conflicts. It is striking that a second transcription factor that engages PAF1c in a similar manner is β-catenin, which drives the oncogenic growth of colorectal tumor cells; like MYC, β-catenin is targeted by the HUWE1 ligase (Dominguez-Brauer et al., 2017; Mosimann et al., 2006; Moyal et al., 2011). We hypothesize, therefore, that targeting PAF1c and its role for the repair of transcription-induced double-strand breaks will open a wide therapeutic window for colorectal and other MYC-driven tumors.



(legend on next page)

STAR★METHODS

Detailed methods are provided in the online version of this paper and include the following:

- **KEY RESOURCES TABLE**
- **RESOURCE AVAILABILITY**
 - Lead contact
 - Materials availability
 - Data and code availability
- **EXPERIMENTAL MODEL AND SUBJECT DETAILS**
 - Cell cultures, primary cells, viral strains
 - Cell line manipulation and generation
- **METHOD DETAILS**
 - General cloning
 - shRNA experiments
 - Protein expression, purification, and in vitro pulldown
 - Immunoblot
 - Immunoprecipitation
 - Chromatin IP without or with reference exogenous genome spike-in (ChIP, ChIP-Rx)
 - Proximity ligation assay
 - siRNA screen
 - BLISS8
 - Cell Cycle Immunofluorescence
 - Confocal microscopy
 - Image processing and colocalization quantification
 - RNA sequencing
 - Flow cytometry
 - Colony formation assay
 - Knockin of the HUWE1 catalytic mutant in HCT116 cells
 - SILAC-based ubiquitin remnant profiling
 - Bioinformatics
- **QUANTIFICATION AND STATISTICAL ANALYSIS**
 - General statistics

SUPPLEMENTAL INFORMATION

Supplemental Information can be found online at <https://doi.org/10.1016/j.molcel.2020.12.035>.

ACKNOWLEDGMENTS

This work was supported by grants from the European Research Council (AuroMYC), the German Research Foundation via the Graduate College (GRK 2243), and the European Fonds for Regional Development (to M.E.). P.B. is supported by the Emmy Noether Program (BE 5342/1-1 and BE5342/1-2). S.M.V. was supported by an EMBO Long-Term Fellowship (ALTF 745-2014). N.P. is supported by the DFG Research Unit FOR2314 “Targeting therapeutic windows in essential cellular processes for tumor therapy” (PO 1458/7-1).

AUTHOR CONTRIBUTIONS

T.E. and D.S. performed ChIP-qPCR, ChIP-Rx, BLISS8, immunoblot and cell-cycle-immunofluorescence assays. T.E. performed RNA-seq, *in vitro* pull-down, shRNA, and MYC-ER/AID assays. D.S. performed the siRNA screen, PLA, and IP assays. D.S. and J.B.H. performed diGLY-SILAC. N.P. and V.A. developed and analyzed the HUWE1 knockin cells. A.B. and E.W. performed the confocal imaging and image analysis. P.G., T.E., and D.S. performed the bioinformatic analyses. P.B., P.G., and M.E. wrote the paper. S.M.V. and P.C. purified and characterized the PAF1 complex, M.M. and J.Z. generated and characterized the MYC-AID system.

DECLARATION OF INTERESTS

The authors declare no competing interests.

Received: May 2, 2020

Revised: October 14, 2020

Accepted: December 16, 2020

Published: January 15, 2021; Corrected online: January 25, 2021

REFERENCES

- Adhikary, S., Marinoni, F., Hock, A., Hulleman, E., Popov, N., Beier, R., Bernard, S., Quarto, M., Capra, M., Goettig, S., et al. (2005). The ubiquitin ligase HectH9 regulates transcriptional activation by Myc and is essential for tumor cell proliferation. *Cell* 123, 409–421.
- Amemiya, H.M., Kundaje, A., and Boyle, A.P. (2019). The ENCODE Blacklist: Identification of Problematic Regions of the Genome. *Sci. Rep.* 9, 9354.
- Annibaldi, D., Whitfield, J.R., Favuzzi, E., Jauset, T., Serrano, E., Cuartas, I., Redondo-Campos, S., Folch, G., González-Juncà, A., Sodik, N.M., et al. (2014). Myc inhibition is effective against glioma and reveals a role for Myc in proficient mitosis. *Nat. Commun.* 5, 4632.
- Aoi, Y., Smith, E.R., Shah, A.P., Rendleman, E.J., Marshall, S.A., Woodfin, A.R., Chen, F.X., Shiekhhattar, R., and Shilatifard, A. (2020). NELF Regulates a Promoter-Proximal Step Distinct from RNA Pol II Pause-Release. *Mol. Cell* 78, 261–274.e5.
- Baluapuri, A., Hofstetter, J., Dudvarski Stankovic, N., Endres, T., Bhandare, P., Vos, S.M., Adhikari, B., Schwarz, J.D., Narain, A., Vogt, M., et al. (2019). MYC Recruits SPT5 to RNA Polymerase II to Promote Processive Transcription Elongation. *Mol. Cell* 74, 674–687.e11.
- Baluapuri, A., Wolf, E., and Eilers, M. (2020). Target gene-independent functions of MYC oncoproteins. *Nat. Rev. Mol. Cell Biol.* 21, 255–267.
- Baranello, L., Wojtowicz, D., Cui, K., Devaiah, B.N., Chung, H.J., Chan-Salis, K.Y., Guha, R., Wilson, K., Zhang, X., Zhang, H., et al. (2016). RNA Polymerase II Regulates Topoisomerase 1 Activity to Favor Efficient Transcription. *Cell* 165, 357–371.
- Beaulieu, M.E., Jauset, T., Massó-Vallés, D., Martínez-Martín, S., Rahl, P., Maltais, L., Zacarias-Fluck, M.F., Casacuberta-Serra, S., Serrano Del Pozo, E., Fiore, C., et al. (2019). Intrinsic cell-penetrating activity propels Omomyc from proof of concept to viable anti-MYC therapy. *Sci. Transl. Med.* 11, eaar5012.
- Büchel, G., Carstensen, A., Mak, K.Y., Roeschert, I., Leen, E., Sumara, O., Hofstetter, J., Herold, S., Kalb, J., Baluapuri, A., et al. (2017). Association with Aurora-A Controls N-MYC-Dependent Promoter Escape and Pause Release of RNA Polymerase II during the Cell Cycle. *Cell Rep.* 21, 3483–3497.

Figure 7. Repair-associated DNA synthesis upon PAF1 depletion

(A) Confocal images of U2OS cells showing EdU incorporation immediately adjacent to γ -H2AX foci in U2OS cells upon constitutive expression shCTR9 and induction of MYC for 24 h. Insert shows Pearson’s correlation constant (PCC). Scale bars: 2 μ m.

(B) Violin plot of Pearson correlation coefficients for co-localization of DNA synthesis and γ -H2AX for each of the experimental conditions (n = 17–21 cells).

(C) Model of our findings.

See also Figure S7.

- Bunch, H., Lawney, B.P., Lin, Y.F., Asaithamby, A., Murshid, A., Wang, Y.E., Chen, B.P., and Calderwood, S.K. (2015). Transcriptional elongation requires DNA break-induced signalling. *Nat. Commun.* **6**, 10191.
- Bywater, M.J., Burkhart, D.L., Straube, J., Sabò, A., Pendino, V., Hudson, J.E., Quaife-Ryan, G.A., Porrello, E.R., Rae, J., Parton, R.G., et al. (2020). Reactivation of Myc transcription in the mouse heart unlocks its proliferative capacity. *Nat. Commun.* **11**, 1827.
- Chen, Y.H., Keegan, S., Kahli, M., Tonzi, P., Fenyó, D., Huang, T.T., and Smith, D.J. (2019). Transcription shapes DNA replication initiation and termination in human cells. *Nat. Struct. Mol. Biol.* **26**, 67–77.
- Chiarle, R., Zhang, Y., Frock, R.L., Lewis, S.M., Molinie, B., Ho, Y.J., Myers, D.R., Choi, V.W., Compagno, M., Malkin, D.J., et al. (2011). Genome-wide translocation sequencing reveals mechanisms of chromosome breaks and rearrangements in B cells. *Cell* **147**, 107–119.
- Clouaire, T., Rocher, V., Lashgari, A., Arnould, C., Aguirrebengoa, M., Biernacka, A., Skrzypczak, M., Aymard, F., Fongang, B., Dojer, N., et al. (2018). Comprehensive Mapping of Histone Modifications at DNA Double-Strand Breaks Deciphers Repair Pathway Chromatin Signatures. *Mol. Cell* **72**, 250–262.e6.
- Courilleau, C., Chailleux, C., Jauneau, A., Grimal, F., Briois, S., Boutet-Robinet, E., Boudsocq, F., Trouche, D., and Canitrot, Y. (2012). The chromatin remodeler p400 ATPase facilitates Rad51-mediated repair of DNA double-strand breaks. *J. Cell Biol.* **199**, 1067–1081.
- Cox, J., and Mann, M. (2008). MaxQuant enables high peptide identification rates, individualized p.p.b.-range mass accuracies and proteome-wide protein quantification. *Nat. Biotechnol.* **26**, 1367–1372.
- Cox, J., Neuhauser, N., Michalski, A., Scheltema, R.A., Olsen, J.V., and Mann, M. (2011). Andromeda: a peptide search engine integrated into the MaxQuant environment. *J. Proteome Res.* **10**, 1794–1805.
- Cramer, P. (2019). Organization and regulation of gene transcription. *Nature* **573**, 45–54.
- Dang, C.V. (2012). MYC on the path to cancer. *Cell* **149**, 22–35.
- de Pretis, S., Kress, T.R., Morelli, M.J., Sabò, A., Locarno, C., Verrecchia, A., Doni, M., Campaner, S., Amati, B., and Pelizzola, M. (2017). Integrative analysis of RNA polymerase II and transcriptional dynamics upon MYC activation. *Genome Res.* **27**, 1658–1664.
- Dominguez-Brauer, C., Khatun, R., Elia, A.J., Thu, K.L., Ramachandran, P., Baniyadi, S.P., Hao, Z., Jones, L.D., Haight, J., Sheng, Y., and Mak, T.W. (2017). E3 ubiquitin ligase Mule targets β -catenin under conditions of hyperactive Wnt signaling. *Proc. Natl. Acad. Sci. USA* **114**, E1148–E1157.
- Easwaran, H., Johnstone, S.E., Van Neste, L., Ohm, J., Mosbrugger, T., Wang, Q., Aryee, M.J., Joyce, P., Ahuja, N., Weisenberger, D., et al. (2012). A DNA hypermethylation module for the stem/progenitor cell signature of cancer. *Genome Res.* **22**, 837–849.
- Ernst, J., and Kellis, M. (2012). ChromHMM: automating chromatin-state discovery and characterization. *Nat. Methods* **9**, 215–216.
- Fellmann, C., Hoffmann, T., Sridhar, V., Hopfgartner, B., Muhar, M., Roth, M., Lai, D.Y., Barbosa, I.A., Kwon, J.S., Guan, Y., et al. (2013). An optimized microRNA backbone for effective single-copy RNAi. *Cell Rep.* **5**, 1704–1713.
- Frank, S.R., Parisi, T., Taubert, S., Fernandez, P., Fuchs, M., Chan, H.M., Livingston, D.M., and Amati, B. (2003). MYC recruits the TIP60 histone acetyltransferase complex to chromatin. *EMBO Rep.* **4**, 575–580.
- Freese, N.H., Norris, D.C., and Loraine, A.E. (2016). Integrated genome browser: visual analytics platform for genomics. *Bioinformatics* **32**, 2089–2095, <https://doi.org/10.1093/bioinformatics/btw069>.
- Fuchs, M., Gerber, J., Drapkin, R., Sif, S., Ikura, T., Ogryzko, V., Lane, W.S., Nakatani, Y., and Livingston, D.M. (2001). The p400 complex is an essential E1A transformation target. *Cell* **106**, 297–307.
- Fuchs, G., Hollander, D., Voichek, Y., Ast, G., and Oren, M. (2014). Cotranscriptional histone H2B monoubiquitylation is tightly coupled with RNA polymerase II elongation rate. *Genome Res.* **24**, 1572–1583.
- Fujinaga, K., Irwin, D., Huang, Y., Taube, R., Kurosu, T., and Peterlin, B.M. (2004). Dynamics of human immunodeficiency virus transcription: P-TEFb phosphorylates RD and dissociates negative effectors from the transactivation response element. *Mol. Cell. Biol.* **24**, 787–795.
- Gabay, M., Li, Y., and Felsher, D.W. (2014). MYC activation is a hallmark of cancer initiation and maintenance. *Cold Spring Harb. Perspect. Med.* **4**, 014241.
- Gerlach, J.M., Furrer, M., Gallant, M., Birkel, D., Baluapuri, A., Wolf, E., and Gallant, P. (2017). PAF1 complex component Leo1 helps recruit *Drosophila* Myc to promoters. *Proc. Natl. Acad. Sci. USA* **114**, E9224–E9232.
- Gothe, H.J., Bouwman, B.A.M., Gusmao, E.G., Piccinno, R., Petrosino, G., Sayols, S., Drechsel, O., Minneker, V., Josipovic, N., Mizi, A., et al. (2019). Spatial Chromosome Folding and Active Transcription Drive DNA Fragility and Formation of Oncogenic MLL Translocations. *Mol. Cell* **75**, 267–283.e12.
- Gregersen, L.H., and Svejstrup, J.Q. (2018). The Cellular Response to Transcription-Blocking DNA Damage. *Trends Biochem. Sci.* **43**, 327–341.
- Gudjonsson, T., Altmeyer, M., Savic, V., Toledo, L., Dinant, C., Grofte, M., Bartkova, J., Poulsen, M., Oka, Y., Bekker-Jensen, S., et al. (2012). TRIP12 and UBR5 suppress spreading of chromatin ubiquitylation at damaged chromosomes. *Cell* **150**, 697–709.
- Guo, J., Li, T., Schipper, J., Nilson, K.A., Fordjour, F.K., Cooper, J.J., Gordán, R., and Price, D.H. (2014). Sequence specificity incompletely defines the genome-wide occupancy of Myc. *Genome Biol.* **15**, 482.
- Hampel, S., Bocek, M.J., Saldivar, J.C., Swigut, T., and Cimprich, K.A. (2017). Transcription-Replication Conflict Orientation Modulates R-Loop Levels and Activates Distinct DNA Damage Responses. *Cell* **170**, 774–786.e19.
- Heidelberger, J.B., Voigt, A., Borisova, M.E., Petrosino, G., Ruf, S., Wagner, S.A., and Beli, P. (2018). Proteomic profiling of VCP substrates links VCP to K6-linked ubiquitylation and c-Myc function. *EMBO Rep.* **19**, e44754.
- Herold, S., Kalb, J., Büchel, G., Ade, C.P., Baluapuri, A., Xu, J., Koster, J., Solvie, D., Carstensen, A., Klotz, C., et al. (2019). Recruitment of BRCA1 limits MYCN-driven accumulation of stalled RNA polymerase. *Nature* **567**, 545–549.
- Ho, J.W., Jung, Y.L., Liu, T., Alver, B.H., Lee, S., Ikegami, K., Sohn, K.A., Minoda, A., Tolstorukov, M.Y., Appert, A., et al. (2014). Comparative analysis of metazoan chromatin organization. *Nature* **512**, 449–452.
- Huang, C.H., Lujambio, A., Zuber, J., Tschaharganeh, D.F., Doran, M.G., Evans, M.J., Kitzing, T., Zhu, N., de Stanchina, E., Sawyers, C.L., et al. (2014). CDK9-mediated transcription elongation is required for MYC addiction in hepatocellular carcinoma. *Genes Dev.* **28**, 1800–1814.
- Hutterer, C., Eickhoff, J., Milbradt, J., Korn, K., Zeitträger, I., Bahsi, H., Wagner, S., Zischinsky, G., Wolf, A., Degenhart, C., et al. (2015). A novel CDK7 inhibitor of the Pyrazolotriazine class exerts broad-spectrum antiviral activity at nanomolar concentrations. *Antimicrob. Agents Chemother.* **59**, 2062–2071.
- Iglewicz, B., and Hoaglin, D.C. (1993). *How to Detect and Handle Outliers* (ASQC Quality Press).
- Jacquet, K., Fradet-Turcotte, A., Avvakumov, N., Lambert, J.P., Roques, C., Pandita, R.K., Paquet, E., Herst, P., Gingras, A.C., Pandita, T.K., et al. (2016). The TIP60 Complex Regulates Bivalent Chromatin Recognition by 53BP1 through Direct H4K20me Binding and H2AK15 Acetylation. *Mol. Cell* **62**, 409–421.
- Jaenicke, L.A., von Eyss, B., Carstensen, A., Wolf, E., Xu, W., Greifenberg, A.K., Geyer, M., Eilers, M., and Popov, N. (2016). Ubiquitin-Dependent Turnover of MYC Antagonizes MYC/PAF1C Complex Accumulation to Drive Transcriptional Elongation. *Mol. Cell* **61**, 54–67.
- Ju, B.G., Lunnyak, V.V., Perissi, V., Garcia-Bassets, I., Rose, D.W., Glass, C.K., and Rosenfeld, M.G. (2006). A topoisomerase II β -mediated dsDNA break required for regulated transcription. *Science* **312**, 1798–1802.
- Kalkat, M., Resetca, D., Lourenco, C., Chan, P.K., Wei, Y., Shiah, Y.J., Vitkin, N., Tong, Y., Sunnerhagen, M., Done, S.J., et al. (2018). MYC Protein Interactome Profiling Reveals Functionally Distinct Regions that Cooperate to Drive Tumorigenesis. *Mol. Cell* **72**, 836–848.e7.
- Kelstrup, C.D., Young, C., Lavallee, R., Nielsen, M.L., and Olsen, J.V. (2012). Optimized fast and sensitive acquisition methods for shotgun proteomics on a quadrupole orbitrap mass spectrometer. *J. Proteome Res.* **11**, 3487–3497.

- Kim, S.Y., Herbst, A., Tworkowski, K.A., Salghetti, S.E., and Tansey, W.P. (2003). Skp2 regulates Myc protein stability and activity. *Mol. Cell* **11**, 1177–1188.
- Kim, J., Guermah, M., McGinty, R.K., Lee, J.S., Tang, Z., Milne, T.A., Shilatfard, A., Muir, T.W., and Roeder, R.G. (2009). RAD6-Mediated transcription-coupled H2B ubiquitylation directly stimulates H3K4 methylation in human cells. *Cell* **137**, 459–471.
- Kim, D., Perte, G., Trapnell, C., et al. (2013). TopHat2: accurate alignment of transcriptomes in the presence of insertions, deletions and gene fusions. *Genome Biol* **14**, <https://doi.org/10.1186/gb-2013-14-4-r36>.
- Kim, J., Woo, A.J., Chu, J., Snow, J.W., Fujiwara, Y., Kim, C.G., Cantor, A.B., and Orkin, S.H. (2010). A Myc network accounts for similarities between embryonic stem and cancer cell transcription programs. *Cell* **143**, 313–324.
- Kim, W., Bennett, E.J., Huttlin, E.L., Guo, A., Li, J., Possemato, A., Sowa, M.E., Rad, R., Rush, J., Comb, M.J., et al. (2011). Systematic and quantitative assessment of the ubiquitin-modified proteome. *Mol. Cell* **44**, 325–340.
- Klein, I.A., Resch, W., Jankovic, M., Oliveira, T., Yamane, A., Nakahashi, H., Di Virgilio, M., Bothmer, A., Nussenzweig, A., Robbiani, D.F., et al. (2011). Translocation-capture sequencing reveals the extent and nature of chromosomal rearrangements in B lymphocytes. *Cell* **147**, 95–106.
- Knobel, P.A., Belotserkovskaya, R., Galanty, Y., Schmidt, C.K., Jackson, S.P., and Stracker, T.H. (2014). USP28 is recruited to sites of DNA damage by the tandem BRCT domains of 53BP1 but plays a minor role in double-strand break metabolism. *Mol. Cell Biol.* **34**, 2062–2074.
- Kouzine, F., Gupta, A., Baranello, L., Wojtowicz, D., Ben-Aissa, K., Liu, J., Przytycka, T.M., and Levens, D. (2013). Transcription-dependent dynamic supercoiling is a short-range genomic force. *Nat. Struct. Mol. Biol.* **20**, 396–403.
- Kress, T.R., Sabò, A., and Amati, B. (2015). MYC: connecting selective transcriptional control to global RNA production. *Nat. Rev. Cancer* **15**, 593–607.
- Langmead, B., and Salzberg, S.L. (2012). Fast gapped-read alignment with Bowtie 2. *Nat. Methods* **9**, 357–359.
- Langmead, B., Trapnell, C., Pop, M., and Salzberg, S.L. (2009). Ultrafast and memory-efficient alignment of short DNA sequences to the human genome. *Genome Biol.* **10**, R25.
- Lans, H., Hoesjmakers, J.H.J., Vermeulen, W., and Marteijn, J.A. (2019). The DNA damage response to transcription stress. *Nat. Rev. Mol. Cell Biol.* **20**, 766–784.
- Li, H., Handsaker, B., Wysoker, A., Fennell, T., Ruan, J., Homer, N., Marth, G., Abecasis, G., and Durbin, R.; 1000 Genome Project Data Processing Subgroup (2009). The Sequence Alignment/Map format and SAMtools. *Bioinformatics* **25**, 2078–2079, <https://doi.org/10.1093/bioinformatics/btp352>.
- Lin, C.Y., Lovén, J., Rahl, P.B., Paranal, R.M., Burge, C.B., Bradner, J.E., Lee, T.I., and Young, R.A. (2012). Transcriptional amplification in tumor cells with elevated c-Myc. *Cell* **151**, 56–67.
- Liu, L., Ulbrich, J., Müller, J., et al. (2012). Deregulated MYC expression induces dependence upon AMPK-related kinase 5. *Nature* **483**, 608–612, <https://doi.org/10.1038/nature10927>.
- Lorenzin, F., Benary, U., Baluapuri, A., Walz, S., Jung, L.A., von Eyss, B., Kisker, C., Wolf, J., Eilers, M., and Wolf, E. (2016). Different promoter affinities account for specificity in MYC-dependent gene regulation. *eLife* **5**, e15161.
- Madabhushi, R., Gao, F., Pfenning, A.R., Pan, L., Yamakawa, S., Seo, J., Rueda, R., Phan, T.X., Yamakawa, H., Pao, P.C., et al. (2015). Activity-Induced DNA Breaks Govern the Expression of Neuronal Early-Response Genes. *Cell* **161**, 1592–1605.
- Magnaghi, P., D'Alessio, R., Valsasina, B., Avanzi, N., Rizzi, S., Asa, D., Gasparri, F., Cozzi, L., Cucchi, U., Orrenius, C., et al. (2013). Covalent and allosteric inhibitors of the ATPase VCP/p97 induce cancer cell death. *Nat. Chem. Biol.* **9**, 548–556.
- Michalski, A., Damoc, E., Lange, O., Denisov, E., Nolting, D., Muller, M., Viner, R., Schwartz, J., Remes, P., Belford, M., et al. (2012). Ultra high resolution linear ion trap Orbitrap mass spectrometer (Orbitrap Elite) facilitates top down LC MS/MS and versatile peptide fragmentation modes. *Mol. Cell Proteomics* **11**, O111.013698.
- Mosimann, C., Hausmann, G., and Basler, K. (2006). Parafibromin/Hyrax activates Wnt/Wg target gene transcription by direct association with beta-catenin/Armadillo. *Cell* **125**, 327–341.
- Moyal, L., Lerenthal, Y., Gana-Weisz, M., Mass, G., So, S., Wang, S.Y., Eppink, B., Chung, Y.M., Shalev, G., Shema, E., et al. (2011). Requirement of ATM-dependent monoubiquitylation of histone H2B for timely repair of DNA double-strand breaks. *Mol. Cell* **41**, 529–542.
- Muhar, M., Ebert, A., Neumann, T., Umkehrer, C., Jude, J., Wieshofer, C., Rescheneder, P., Lipp, J.J., Herzog, V.A., Reichholf, B., et al. (2018). SLAM-seq defines direct gene-regulatory functions of the BRD4-MYC axis. *Science* **360**, 800–805.
- Murr, R., Loizou, J.I., Yang, Y.G., Cuenin, C., Li, H., Wang, Z.Q., and Herceg, Z. (2006). Histone acetylation by Trapp-Tip60 modulates loading of repair proteins and repair of DNA double-strand breaks. *Nat. Cell Biol.* **8**, 91–99.
- Nakamura, K., Kato, A., Kobayashi, J., Yanagihara, H., Sakamoto, S., Oliveira, D.V., Shimada, M., Tauchi, H., Suzuki, H., Tashiro, S., et al. (2011). Regulation of homologous recombination by RNF20-dependent H2B ubiquitination. *Mol. Cell* **41**, 515–528.
- Nie, Z., Hu, G., Wei, G., Cui, K., Yamane, A., Resch, W., Wang, R., Green, D.R., Tessarollo, L., Casellas, R., et al. (2012). c-Myc is a universal amplifier of expressed genes in lymphocytes and embryonic stem cells. *Cell* **151**, 68–79.
- Oliveira, D.V., Kato, A., Nakamura, K., Ikura, T., Okada, M., Kobayashi, J., Yanagihara, H., Saito, Y., Tauchi, H., and Komatsu, K. (2014). Histone chaperone FACT regulates homologous recombination by chromatin remodeling through interaction with RNF20. *J. Cell Sci.* **127**, 763–772.
- Olson, C.M., Jiang, B., Erb, M.A., Liang, Y., Doctor, Z.M., Zhang, Z., Zhang, T., Kwiatkowski, N., Boukhali, M., Green, J.L., et al. (2018). Pharmacological perturbation of CDK9 using selective CDK9 inhibition or degradation. *Nat. Chem. Biol.* **14**, 163–170.
- Orlando, D.A., Chen, M.W., Brown, V.E., Solanki, S., Choi, Y.J., Olson, E.R., Fritz, C.C., Bradner, J.E., and Guenther, M.G. (2014). Quantitative ChIP-Seq normalization reveals global modulation of the epigenome. *Cell Rep.* **9**, 1163–1170.
- Orthwein, A., Noordermeer, S.M., Wilson, M.D., Landry, S., Enchev, R.I., Sherker, A., Munro, M., Pinder, J., Salsman, J., Deltre, G., et al. (2015). A mechanism for the suppression of homologous recombination in G1 cells. *Nature* **528**, 422–426.
- Peter, S., Bultinck, J., Myant, K., Jaenicke, L.A., Walz, S., Müller, J., Gmachl, M., Treu, M., Boehmelt, G., Ade, C.P., et al. (2014). Tumor cell-specific inhibition of MYC function using small molecule inhibitors of the HUWE1 ubiquitin ligase. *EMBO Mol. Med.* **6**, 1525–1541.
- Poli, J., Gerhold, C.B., Tosi, A., Hustedt, N., Seeber, A., Sack, R., Herzog, F., Pasero, P., Shimada, K., Hopfner, K.P., and Gasser, S.M. (2016). Mec1, INO80, and the PAF1 complex cooperate to limit transcription replication conflicts through RNAPII removal during replication stress. *Genes Dev.* **30**, 337–354.
- Popov, N., Wanzel, M., Madiredjo, M., Zhang, D., Beijersbergen, R., Bernards, R., Moll, R., Elledge, S.J., and Eilers, M. (2007). The ubiquitin-specific protease USP28 is required for MYC stability. *Nat. Cell Biol.* **9**, 765–774.
- Puc, J., Kozbial, P., Li, W., Tan, Y., Liu, Z., Suter, T., Ohgi, K.A., Zhang, J., Aggarwal, A.K., and Rosenfeld, M.G. (2015). Ligand-dependent enhancer activation regulated by topoisomerase-I activity. *Cell* **160**, 367–380.
- Qiao, X., Liu, Y., Prada, M.L., Mohan, A.K., Gupta, A., Jaiswal, A., Sharma, M., Merisaari, J., Haikala, H.M., Talvinen, K., et al. (2020). *UBR5* Is Coamplified with *MYC* in Breast Tumors and Encodes an Ubiquitin Ligase That Limits MYC-Dependent Apoptosis. *Cancer Res.* **80**, 1414–1427.
- Quinlan, A.R., and Hall, I.M. (2010). BEDTools: a flexible suite of utilities for comparing genomic features. *Bioinformatics* **26**, 841–842.
- Rahl, P.B., Lin, C.Y., Seila, A.C., Flynn, R.A., McCuine, S., Burge, C.B., Sharp, P.A., and Young, R.A. (2010). c-Myc regulates transcriptional pause release. *Cell* **141**, 432–445.

- Ramírez, F., Ryan, D.P., Grüning, B., Bhardwaj, V., Kilpert, F., Richter, A.S., Heyne, S., Dündar, F., and Manke, T. (2016). deepTools2: a next generation web server for deep-sequencing data analysis. *Nucleic Acids Res.* *44* (W1), W160–W165.
- Robinson, M.D., McCarthy, D.J., and Smyth, G.K. (2010). edgeR: a Bioconductor package for differential expression analysis of digital gene expression data. *Bioinformatics* *26*, 139–140, <https://doi.org/10.1093/bioinformatics/btp616>.
- Sabò, A., Kress, T.R., Pelizzola, M., de Pretis, S., Gorski, M.M., Tesi, A., Morelli, M.J., Bora, P., Doni, M., Verrecchia, A., et al. (2014). Selective transcriptional regulation by Myc in cellular growth control and lymphomagenesis. *Nature* *511*, 488–492.
- Shen, L., Shao, N., Liu, X., and Nestler, E. (2014). ngs.plot: quick mining and visualization of next-generation sequencing data by integrating genomic databases. *BMC Genomics* *15*, 284.
- Singh, S., Szlachta, K., Manukyan, A., Raimer, H.M., Dinda, M., Bekiranov, S., and Wang, Y.H. (2020). Pausing sites of RNA polymerase II on actively transcribed genes are enriched in DNA double-stranded breaks. *J. Biol. Chem.* *295*, 3990–4000.
- Smith, T., Heger, A., and Sudbery, I. (2017). UMI-tools: modeling sequencing errors in Unique Molecular Identifiers to improve quantification accuracy. *Genome Res.* *27*, 491–499.
- Sondalle, S.B., Longrich, S., Ogawa, L.M., Sung, P., and Baserga, S.J. (2019). Fanconi anemia protein FANCI functions in ribosome biogenesis. *Proc. Natl. Acad. Sci. USA* *116*, 2561–2570.
- Soucek, L., Whitfield, J.R., Sodik, N.M., Massó-Vallés, D., Serrano, E., Karnezis, A.N., Swigart, L.B., and Evan, G.I. (2013). Inhibition of Myc family proteins eradicates KRas-driven lung cancer in mice. *Genes Dev.* *27*, 504–513.
- Sun, X.X., He, X., Yin, L., Komada, M., Sears, R.C., and Dai, M.S. (2015). The nucleolar ubiquitin-specific protease USP36 deubiquitinates and stabilizes c-Myc. *Proc. Natl. Acad. Sci. USA* *112*, 3734–3739.
- Tasselli, L., Xi, Y., Zheng, W., Tennen, R.I., Odrowaz, Z., Simeoni, F., Li, W., and Chua, K.F. (2016). SIRT6 deacetylates H3K18ac at pericentric chromatin to prevent mitotic errors and cellular senescence. *Nat. Struct. Mol. Biol.* *23*, 434–440.
- Tesi, A., de Pretis, S., Furlan, M., Filipuzzi, M., Morelli, M.J., Andronache, A., Doni, M., Verrecchia, A., Pelizzola, M., Amati, B., and Sabò, A. (2019). An early Myc-dependent transcriptional program orchestrates cell growth during B-cell activation. *EMBO Rep.* *20*, e47987.
- Van Oss, S.B., Shirra, M.K., Bataille, A.R., Wier, A.D., Yen, K., Vinayachandran, V., Byeon, I.L., Cucinotta, C.E., Héroux, A., Jeon, J., et al. (2016). The Histone Modification Domain of Paf1 Complex Subunit Rtf1 Directly Stimulates H2B Ubiquitylation through an Interaction with Rad6. *Mol. Cell* *64*, 815–825.
- Van Oss, S.B., Cucinotta, C.E., and Arndt, K.M. (2017). Emerging Insights into the Roles of the Paf1 Complex in Gene Regulation. *Trends Biochem. Sci.* *42*, 788–798.
- Venkitaraman, A.R. (2014). Cancer suppression by the chromosome custodians, BRCA1 and BRCA2. *Science* *343*, 1470–1475.
- von der Lehr, N., Johansson, S., Wu, S., Bahram, F., Castell, A., Cetinkaya, C., Hydbring, P., Weidung, I., Nakayama, K., Nakayama, K.I., et al. (2003). The F-box protein Skp2 participates in c-Myc proteosomal degradation and acts as a cofactor for c-Myc-regulated transcription. *Mol. Cell* *11*, 1189–1200.
- Vos, S.M., Farnung, L., Boehning, M., Wigge, C., Linden, A., Urlaub, H., and Cramer, P. (2018a). Structure of activated transcription complex Pol II-DSIF-PAF-SPT6. *Nature* *560*, 607–612.
- Vos, S.M., Farnung, L., Urlaub, H., and Cramer, P. (2018b). Structure of paused transcription complex Pol II-DSIF-NELF. *Nature* *560*, 601–606.
- Walz, S., Lorenzin, F., Morton, J., Wiese, K.E., von Eyss, B., Herold, S., Rycak, L., Dumay-Odelot, H., Karim, S., Bartkuhn, M., et al. (2014). Activation and repression by oncogenic MYC shape tumour-specific gene expression profiles. *Nature* *511*, 483–487.
- Wen, H., Li, Y., Xi, Y., Jiang, S., Stratton, S., Peng, D., Tanaka, K., Ren, Y., Xia, Z., Wu, J., et al. (2014). ZMYND11 links histone H3.3K36me3 to transcription elongation and tumour suppression. *Nature* *508*, 263–268.
- Wiese, K.E., Haikala, H.M., von Eyss, B., Wolf, E., Esnault, C., Rosenwald, A., Treisman, R., Klefström, J., and Eilers, M. (2015). Repression of SRF target genes is critical for Myc-dependent apoptosis of epithelial cells. *EMBO J.* *34*, 1554–1571, <https://doi.org/10.15252/embj.201490467>.
- Xu, G., Paige, J.S., and Jaffrey, S.R. (2010). Global analysis of lysine ubiquitination by ubiquitin remnant immunoprecipitation. *Nat. Biotechnol.* *28*, 868–873.
- Yan, W.X., Mirzazadeh, R., Garnerone, S., Scott, D., Schneider, M.W., Kallas, T., Custodio, J., Wernersson, E., Li, Y., Gao, L., et al. (2017). BLISS is a versatile and quantitative method for genome-wide profiling of DNA double-strand breaks. *Nat. Commun.* *8*, 15058.
- Zhang, Y., Liu, T., Meyer, C.A., et al. (2008). Model-based Analysis of ChIP-Seq (MACS). *Genome Biol.* *9*, <https://doi.org/10.1186/gb-2008-9-9-r137>.
- Zhang, D., Zaugg, K., Mak, T.W., and Elledge, S.J. (2006). A role for the deubiquitinating enzyme USP28 in control of the DNA-damage response. *Cell* *126*, 529–542.

STAR★METHODS

KEY RESOURCES TABLE

REAGENT or RESOURCE	SOURCE	IDENTIFIER
Antibodies		
Mono- & polyubiquitinated conjugates (FK2)	Enzo Life Sciences	BML-PW8810; RRID: AB_10541840
Mouse monoclonal anti-Pol II (A-10)	Santa Cruz Biotechnology	Cat#sc-17798; RRID: AB_677355
Mouse monoclonal anti-Pol II (F-12)	Santa Cruz Biotechnology	Cat#sc-55492; RRID: AB_630203
Rabbit monoclonal anti-MYC (clone Y69)	Abcam	Cat# ab32072; RRID: AB_731658
Mouse Monoclonal anti-MYC (C33)	Santa Cruz Biotechnology	Cat#sc-42; RRID: AB_2282408
Rabbit polyclonal anti-phospho-Ser2-RNAPII	Abcam	Cat# ab5095; RRID: AB_304749
Mouse monoclonal anti-RNAPII	MBL International	Cat# MABI0601; RRID: AB_2728735
Rabbit polyclonal anti-Histone H2B antibody	Abcam	Ab1790; RRID: AB_302612
Rabbit polyclonal anti-HUWE1/Mule antibody	Abcam	Ab70161; RRID: AB_1209511
Rabbit polyclonal anti-CTR9	Novus Biologicals	NB100-68205; RRID: AB_11002327
Rabbit polyclonal anti-CTR9	Bethyl Laboratories	A301-395; RRID: AB_960973
Rabbit polyclonal anti-Parafibromin (CDC73)	Bethyl Laboratories	A300-171A; RRID: AB_2078660
Rabbit polyclonal anti-PAF1	Abcam	Ab20662; RRID: AB_2159769
Rabbit polyclonal anti-LEO1	Novus Biologicals	NB600-276; RRID: AB_2281237
Goat polyclonal anti-GST	GE Healthcare/Sigma-Aldrich	Cat#GE27-4577-01; RRID: AB_771432 Lot: 362611
Rabbit monoclonal Ubiquityl-Histone H2B (Lys120) (D11) XP®	Cell Signaling Technology	Cat#5546; RRID: AB_10693452
Mouse monoclonal anti-VCL	Sigma-Aldrich	Cat#V9131; RRID: AB_477629
Mouse monoclonal anti-phospho-Ser5-RNAPII	Biolegend	Cat#904001; RRID: AB_2565036
Rabbit polyclonal anti- CDK2	Santa Cruz Biotechnology	Cat#sc-163; RRID: AB_631215
Rabbit polyclonal anti-CHK1(FL-476)	Santa Cruz Biotechnology	Cat#sc-7898; RRID: AB_2229488
Rabbit polyclonal anti-phospho-Chk1 (Ser345) (133D3)	Cell Signaling Technology	Cat#2348; RRID: AB_331212
Rabbit polyclonal anti- phospho-Histone H2A.X (Ser 139)	Cell Signaling Technology	Cat#2577; RRID: AB_2118010
Rabbit polyclonal anti-KAP1 (phospho S824)	Abcam	Cat#ab70369; RRID: AB_1209417
Rabbit polyclonal anti- KAP1	Bethyl Laboratories	Cat#A300-274A; RRID: AB_185559
Rabbit monoclonal Anti-TH1L (D5G6W) (NELFC)	Cell Signaling Technology	Cat#12265S; Lot:1; RRID: AB_2797862
Mouse monoclonal FITC anti-BrdU (clone 3D4)	Biozol / BioLegend	Cat#364104; RRID: AB_2564481
Donkey polyclonal anti-goat IgG-HRP secondary antibody	Santa Cruz Biotechnology	Cat#sc-2020; RRID: AB_631728
ECL-Anti-rabbit IgG Horseradish Peroxidase	GE Healthcare / Fisher Scientific GmbH	Cat#1079-4347 / GEHENA934; RRID: AB_2650489
ECL-Anti-mouse IgG Horseradish Peroxidase	GE Healthcare / Fisher Scientific GmbH	Cat#1019-6124 / GEHENA931

(Continued on next page)

Continued

REAGENT or RESOURCE	SOURCE	IDENTIFIER
IRDye 800CW Donkey anti-Rabbit IgG (H + L)	LI-COR Biosciences	Cat#926-32213; RRID: AB_621848
IRDye 680RD Donkey anti-Mouse IgG (H + L)	LI-COR Biosciences	Cat#926-68072; RRID: AB_10953628
Goat anti-Mouse IgG (H+L) Highly Cross-Adsorbed Secondary Antibody, Alexa Fluor 488	Thermo Fisher Scientific	Cat#A-11029; RRID: AB_138404
Goat anti-Mouse IgG (H+L) Highly Cross-Adsorbed Secondary Antibody, Alexa Fluor 568	Thermo Fisher Scientific	Cat#A-11004; RRID: AB_2534072
Bacterial and virus strains		
pRRL-SFFV-IRES-Hygro	(Wiese et al., 2015)	N/A
pRRL-SFFV-MYC-IRES-Hygro	(Wiese et al., 2015)	N/A
pRRL-SFFV-OsTir1_3x_Myc_tag-T2A-eBFP2	Muhar et al., 2018	N/A
pInducer10 shCDC73-3	This paper	N/A
pInducer10 shCTR9-3	This paper	N/A
pGIPZ shCDC73-3	This paper	N/A
pGIPZ shCDC73-4	This paper	N/A
pGIPZ shCTR9-3	This paper	N/A
pGIPZ shCTR9-5	This paper	N/A
Chemicals, peptides, and recombinant proteins		
MG-132	Calbiochem / Merck	Cat#474790-20MG
HUWE1-Inhibitor BI8626	ProbeChem	N/A
Doxycycline hyclate	Sigma-Aldrich	Cat#D9891-10G
Indole-3-acetic acid sodium salt	Sigma-Aldrich	Cat# I5148-2G
Hoechst 33342	Sigma-Aldrich	Cat#B2261-25MG
5-Ethynyl-2'-deoxyuridine (5-EdU)	Jena Bioscience	Cat#CLK-N001-100
AF647-Picolyl-Azide	Jena Bioscience	Cat#CLK-1300-1
Lipofectamine RNAiMAX Transfection Reagent	Thermo Fischer Scientific	Cat#13778-150
Dynabeads Protein A	Thermo Fisher Scientific	Cat#10001D
Dynabeads Protein G	Thermo Fisher Scientific	Cat#10003D
Dynabeads® MyOne Streptavidin T1	Thermo Fisher Scientific	Cat#65601
Etoposide	Sigma-Aldrich	Cat#E1383
4-Hydroxytamoxifen	Sigma-Aldrich	Cat#H7904
Opti-MEM I	Thermo Fischer Scientific	Cat#31985-047
Propidium iodide	Sigma-Aldrich	Cat#81845
Protease inhibitor cocktail	Sigma-Aldrich	Cat#P8340
Phosphatase inhibitor cocktail 2	Sigma-Aldrich	Cat#P5726
Phosphatase inhibitor cocktail 3	Sigma-Aldrich	Cat#P0044
NuPAGE LDS Sample Buffer (4X)	Sigma-Aldrich	Cat#NP0007
Pierce DTT (Dithiothreitol), No-Weigh Format	Thermo Fisher Scientific	Cat#20291
Benzonase nuclease purity > 99% 25U/μl	Merck Millipore	Cat#70664-3
InstantBlue(TM) Safe Coomassie Stain	Sigma-Aldrich	Cat#ISB1L-1L
Proteinase K	Roth	Cat#7528.2
RNase A	Roth	Cat#7156.1

(Continued on next page)

REAGENT or RESOURCE	SOURCE	IDENTIFIER
16% Paraformaldehyde (Formaldehyde) Aqueous Solution, EM Grade	Science Services GmbH	Cat#E15710
Penicillin-Streptomycin	Sigma-Aldrich	Cat#P4333-100ML
HiMark pre-stained HMW STD	Thermo Fisher Scientific	Cat#LC5699
UltraPure BSA (50 mg/mL)	Thermo Fisher Scientific	Cat#AM2616
Polybrene	Sigma-Aldrich	Cat#H9268
Protamine sulfate	Sigma-Aldrich	Cat#P3369
Alexa Fluor568 Phalloidin	Thermo Fisher Scientific	Cat#A12380
N-Ethylmaleinimid	Sigma-Aldrich	Cat#E3876
Puromycin	InvivoGen	Cat#70664-3
Hygromycin B Gold solution	InvivoGen	Cat#ant-hg-05
Blasticidin	InvivoGen	Cat#ant-bl-05
CutSmart® Buffer	New England Biolabs	Cat#B7204S
T4 DNA Ligase Buffer	New England Biolabs	Cat#B0202S
Agencourt AMPure XP Beads	Beckman Coulter	Cat#A63881
Agencourt RNAClean XP Beads	Beckman Coulter	Cat#A63987
LDC4297	Selleckchem / Biozol	Cat#SEL-S7992
NVP-2	Tocris/Bio-Techne	Cat#6535/5
Odyssey Blocking Buffer in TBS	LI-COR Biosciences	Cat#927-50000
Glutathione Sepharose 4B	GE Healthcare / VWR International	Cat#17075601
L-Glutathion reduced, cell culture tested	Sigma-Aldrich	Cat#G6013-5G
Fugene	Promega	Cat#E2311
Critical commercial assays		
Duolink <i>In Situ</i> PLA Probe Anti-Rabbit PLUS, Affinity purified Donkey anti-Rabbit IgG (H+L)	Sigma-Aldrich	Cat#DUO92002; RRID: AB_2810940
Duolink <i>In Situ</i> PLA Probe Anti-Mouse MINUS, Affinity purified Donkey anti-Mouse IgG (H+L)	Sigma-Aldrich	Cat#DUO92004; RRID: AB_2713942
Duolink <i>In Situ</i> Wash Buffers, Fluorescence	Sigma-Aldrich	Cat#DUO82049
Duolink <i>In Situ</i> Detection Reagents Green	Sigma-Aldrich	Cat#DUO92014
NGS Fragment High Sensitivity Analysis Kit, 1-6,000 bp, 500 samples	Agilent	DNF-474-0500
Standard Sensitivity RNA Analysis Kit (15nt), 500 samples	Agilent	DNF-471-0500
RNeasy Mini Kit	QIAGEN	Cat#74106
MinElute PCR Purification Kit	QIAGEN	Cat#28006
QIAquick PCR Purification Kit	QIAGEN	Cat#28106
QIAquick Gel Extraction Kit	QIAGEN	Cat#28704
NEBNext Ultra RNA Library Prep Kit for Illumina	New England Biolabs	Cat#E7530S
NEBNext Poly(A) mRNA Magnetic Isolation Modul	New England Biolabs	Cat#E7490L
NEBNext ChIP-Seq Prep Master Mix Set for Illumina	New England Biolabs	Cat#E6240S
NEBNext Ultra II DNA Library Prep	New England Biolabs	Cat# E7103L
NEBNext Multiplex Small RNA Library Prep Kit	New England Biolabs	Cat#E7560S
NextSeq 500/550 High Output Kit v2 (75cycles)	Illumina	FC-404-2005

(Continued on next page)

Continued

REAGENT or RESOURCE	SOURCE	IDENTIFIER
Quant-iT Pico Green	Thermo Fischer Scientific	Cat#P7589
AsiSI	New England Biolabs	Cat# R0630
Absolute QPCR Mix, SYBR Green, no ROX	Thermo Fischer Scientific	Cat#AB-1158/B
Quick Blunting Kit	New England Biolabs	Cat#E1201L
T4 DNA Ligase, conc.	New England Biolabs	Cat#M0202M
T4 RNA Ligase 2, truncated	New England Biolabs	Cat#M0242L
NEBNext High-Fidelity 2X PCR Master Mix	New England Biolabs	Cat#M0541L
MEGAscript T7 Transcription Kit	Thermo Fischer Scientific	Cat#AM1334
SuperScript III Reverse Transcriptase	Thermo Fischer Scientific	Cat#T18080044
RNaseOUT Recombinant Ribonuclease Inhibitor	Thermo Fischer Scientific	Cat#10777019
ON-TARGETplus Non-targeting Pool	Horizon Discovery Group	Cat#D-001810-10-50
ON-TARGETplus Set of Four siRNA Library-Human Ubiquitin Conjugation Subset 1	Dharmacon	GU-105615 Lot 11107
ON-TARGETplus Set of Four siRNA Library-Human Ubiquitin Conjugation Subset 2	Dharmacon	GU-105625 Lot 11108
ON-TARGETplus SMARTpool® siRNA Library - Human Ubiquitin Conjugation Subset 3	Dharmacon	GU-105635 Lot 11117
PTMScan Ubiquitin Remnant Motif (K-ε-GG) Kit	Cell Signaling Technology	Cat#5562

Deposited data

Sequencing Data	This paper	GSE150217
Raw imaging data	This paper	10.17632/n4rr8ck4w3.1

Experimental models: cell lines

NIH 3T3	ATCC	CVCL_0594
U2OS	ATCC	N/A
HEK293TN	ATCC	CRT-11268
U2OS MYC-Tet-On	Walz et al., 2014	N/A
U2OS MYC-ER	Liu et al., 2012	N/A
K562 MYC-Aid	Muhar et al., 2018	N/A

Oligonucleotides

Primer ChIP qPCR NCL_f CTACCACCCTCATCTGAATCC	Baluapuri et al., 2019	N/A
Primer ChIP qPCR NCL_r TTGTCTCGCTGGGAAAGG	Baluapuri et al., 2019	N/A
Primer ChIP qPCR NegReg_f TTTTCTCACATTGCCCTGT	Baluapuri et al., 2019	N/A
Primer ChIP qPCR NegReg_r TCAATGCTGTACCAGGCAAA	Baluapuri et al., 2019	N/A
Primer ChIP qPCR GNL3 f GTGACGCTCGTCAGTGG	Jaenicke et al., 2016	N/A
Primer ChIP qPCR GNL3 rCA TATTGGCTGTAGAAGGAAGC	Jaenicke et al., 2016	N/A
Primer ChIP qPCR NPM1 f TTCACCGGAAGCATGG	Jaenicke et al., 2016	N/A
Primer ChIP qPCR NPM1 r CACGCGAGGTAAGTCTACG	Jaenicke et al., 2016	N/A
Primer ChIP qPCR IFRD1 r CGTGGTTTGGCTACTGAACT	This paper	N/A

(Continued on next page)

REAGENT or RESOURCE	SOURCE	IDENTIFIER
Primer ChIP qPCR IFRD1 f CCTGTCCCGACACACTCTC	This paper	N/A
Primer ChIP qPCR CHMP2A r CAAGGTGGTGTGGAGACCT	This paper	N/A
Primer ChIP qPCR CHMP2A f GGGGATCCCAGAAAGAGAAG	This paper	N/A
shCDC73 human mirE3 TGCTGTTG ACAGTGAGCGCCAGCGATCTACT CAAGTCAAATAGTGAAGCCACAGA TGTATTTGACTTGAGTAGATCGCTG ATGCCTACTGCCTCGGA	Fellmann et al., 2013	N/A
shCDC73 human mirE4TGCTGTTG ACAGTGAGCGCCAGGTACATGGT AAAGCATAATAGTGAAGCCACAGA TGTATTATGCTTTACCATGTACCTG TTGCCTACTGCCTCGGA	Fellmann et al., 2013	N/A
shCTR9 human mirE3TGCTGTTG ACAGTGAGCGCTCGGATGAGGA TAAACTTAAATAGTGAAGCCACAG ATGTATTTAAGTTTATCCTCATCC GAATGCCTACTGCCTCGGA	Fellmann et al., 2013	N/A
shCTR9 human mirE5TGCTGTTGA CAGTGAGCGAAAGCAACAAAAGA GAAGAAAATAGTGAAGCCACAGA TGTATTTTCTTCTTTTTGTTGCTT CTGCCTACTGCCTCGGA	Fellmann et al., 2013	N/A
MYC-f (pGex4T3)CCCGAATTCG CCCCTCAACGTTAGCTTC	Baluapuri et al., 2019	N/A
MYC-r (pGex4T3)GGGCTCGAGT CAGTTCGGGCTGCCGCTGTCT	Baluapuri et al., 2019	N/A
A1_Bottom [P]GCGTGATGNNNNNNNN GATCGTCGGACTGTAGAACTCTGAAC CCCTATAGTGAGTCGTATTACCGG CCTCAATCGAA	Yan et al., 2017	N/A
A1_Top CGATTGAGGCCGGTAAT ACGACTCACTATAGGGGTTCAGA GTTCTACAGTCCGACGATCNNN NNNNNCATCACGC	Yan et al., 2017	N/A
A2_Bottom [P]GGAACGACNNNNNNNNG ATCGTCGGACTGTAGAACTCTGA ACCCCTATAGTGAGTCGTATTACC GGCCTCAATCGAA	Yan et al., 2017	N/A
A2_TopCGATTGAGGCCGGTAATACG ACTCACTATAGGGGTTCCAGAG TTCTACAGTCCGACGATCNNNN NNNNGTCGTTCC	Yan et al., 2017	N/A
A3_Bottom [P]GATCATCANNNNNNNN GATCGTCGGACTGTAGAACTCTGA ACCCCTATAGTGAGTCGTATTACC GGCCTCAATCGAA	Yan et al., 2017	N/A
A3_TopCGATTGAGGCCGGTAATACG ACTCACTATAGGGGTTCCAGAGTTC TACAGTCCGACGATCNNNN NNNNTGATGATC	Yan et al., 2017	N/A

(Continued on next page)

Continued

REAGENT or RESOURCE	SOURCE	IDENTIFIER
A4_Bottom [P]GATGTCGTNNNNN NNNGATCGTCGGACTGTAGAA CTCTGAACCCCTATAGTGAGTC GTATTACCGGCCTCAATCGAA	Yan et al., 2017	N/A
A4_TopCGATTGAGGCCGGTAATA CGACTCACTATAGGGGTTCA GAGTTCTACAGTCCGACGATC NNNNNNNNACGACATC	Yan et al., 2017	N/A
A5_Bottom [P]GGATGATGNNNNNNNN GATCGTCGGACTGTAGAACTCTG AACCCCTATAGTGAGTCGTAT TACCGGCCTCAATCGAA	Yan et al., 2017	N/A
A5_TopCGATTGAGGCCGGTA ATACGACTCACTATAGGGG TTCAGAGTTCTACAGTCCGAC GATCNNNNNNNNCATCATCC	Yan et al., 2017	N/A
A6_Bottom [P]GCGGTCGTNNNN NNNGATCGTCGGACTGTAG AACTCTGAACCCCTATAGTGAGTC GTATTACCGGCCTCAATCGAA	Yan et al., 2017	N/A
A6_TopCGATTGAGGCCGGTAATAC GACTCACTATAGGGGTTAGAGTT CTACAGTCCGACGATCNNNNNN NNACGACCGC	Yan et al., 2017	N/A
RPI_01CAAGCAGAAGACGGCA TACGAGATCGAGTAATGTGACT GGAGTTCCCTGGCACCCGAGAATTCCA	This paper	N/A
RPI_02CAAGCAGAAGACGGCATAACGAGA TTCTCCGGAGTGACTGGAGTTCCCT TGGCACCCGAGAATTCCA	This paper	N/A
RPI_03CAAGCAGAAGACGGCATAACGAG ATAATGAGCGGTGACTGGAGTTCC TTGGCACCCGAGAATTCCA	This paper	N/A
RPI_04CAAGCAGAAGACGGCATAACGA GATGGAATCTCGTGACTGGAGTT CCTTGGCACCCGAGAATTCCA	This paper	N/A
RPI_05CAAGCAGAAGACGGCATAACG AGATTTCTGAATGTGACTGGAGTT CCTTGGCACCCGAGAATTCCA	This paper	N/A
RPI_06CAAGCAGAAGACGGCATAAC GAGATACGAATTCGTGACTGGA GTTCCCTGGCACCCGAGAATTCCA	This paper	N/A
RPI_07CAAGCAGAAGACGGCATAAC GAGATAGCTTCAGGTGACTGGAG TTCCTTGGCACCCGAGAATTCCA	This paper	N/A
RPI_08CAAGCAGAAGACGGCA TACGAGATGCGCATTAGTGACT GGAGTTCCCTGGCACCCGAGAATTCCA	This paper	N/A
RPI_09CAAGCAGAAGACGGCA TACGAGATCATAGCCGGTGACTG GAGTTCCCTGGCACCCGAGAATTCCA	This paper	N/A
RPI_10CAAGCAGAAGACGGCATA CGAGATTCGCGGAGTGACTGGA GTTCCCTGGCACCCGAGAATTCCA	This paper	N/A

(Continued on next page)

<i>Continued</i>		
REAGENT or RESOURCE	SOURCE	IDENTIFIER
RPI_11CAAGCAGAAGACGGCATA GAGATGCGCGAGAGTGACTGGAG TTCCTTGGCACCCGAGAATTCCA	This paper	N/A
RPI_12CAAGCAGAAGACGGCATA CGAGATCTATCGCTGTGACTGGA GTTCTTGGCACCCGAGAATTCCA	This paper	N/A
RA3TGGAAATTCTCGGGTGCCAAGG	Illumina	N/A
RTPGCCTTGGCACCCGAGAATTCCA	Illumina	N/A
RP1AATGATACGGCGACCACCGA GATCTACACGTTTCCAGAGTTCTA CAGTCCGA	Illumina	N/A
SiHUWE1GAGUUUGGAG UUUGUGAAG[dT][dT]	Heidelberger et al., 2018	N/A
sgRNA HUWE1_1AAGGC CCTGCCAACTCCGT	This paper	N/A
sgRNA HUWE1_2CATG CTACTGTTGGCTATCC	This paper	N/A
Recombinant DNA		
pGex-4T3	Pharmacia	N/A
pGex-4T3-MYC1-163	Balupuri et al., 2019	N/A
pGex-4T3-MYC1-163 DMBI	This Paper	N/A
pGex-4T3-MYC1-163 DMBII	This Paper	N/A
pInducer10	Trono Laboratory	N/A
pGIPZ	Dharmacon	N/A
psPAX2	Trono Laboratory	Addgene 12260
pMD2.G	Trono Laboratory	Addgene 12259
PX459	Zhang Laboratory	Addgene 62988
Software and algorithms		
FASTQ Generation software v1.0.0	Illumina	http://www.illumina.com
FastQC v0.11.3	http://www.bioinformatics.babraham.ac.uk/projects/fastqc/	https://www.bioinformatics.babraham.ac.uk/projects/fastqc/
Tophat v2.1.0	(Kim et al., 2013)	https://ccb.jhu.edu/software/tophat/index.shtml
Bowtie v1.2	Langmead et al., 2009	http://bowtie-bio.sourceforge.net/index.shtml
Bowtie v2.3.2	Langmead and Salzberg, 2012	http://bowtie-bio.sourceforge.net/bowtie2/index.shtml
MACS v1.4.1	(Zhang et al., 2008)	https://github.com/macs3-project/MACS
BEDtools v2.26.0	Quinlan and Hall, 2010	https://bedtools.readthedocs.io/en/latest/
SAMtools v1.3	(Li et al., 2009)	http://www.htslib.org/
NGSplot v2.61	Shen et al., 2014	https://github.com/shenlab-sinai/ngsplot
Integrated Genome Browser v9.0.0	(Freese et al., 2016)	https://bioviz.org/
GraphPad Prism v5/6.0 for Mac	GraphPad software	https://www.graphpad.com/scientific-software/prism/
Harmony High Content Imaging and Analysis Software	PerkinElmer	https://www.perkinelmer.de/product/harmony-4-8-office-hh17000001
StepOne software v2.3	StepOne	https://www.thermofisher.com/us/en/home/technical-resources/software-downloads/StepOne-and-StepOnePlus-Real-Time-PCR-System.html

(Continued on next page)

Continued

REAGENT or RESOURCE	SOURCE	IDENTIFIER
BD FACSDIVA Software v6.1.2	BD	https://www.bdbiosciences.com/us/instruments/research/software/flow-cytometry-acquisition/bd-facsdiva-software/m/111112/overview
EdgeR	(Robinson et al., 2010)	https://bioconductor.org/packages/release/bioc/html/edgeR.html
R version 3.6.3	The R Foundation	https://www.R-project.org/
UMI-tools v1.0.0	Smith et al., 2017	https://umi-tools.readthedocs.io/en/latest/index.html
DeepTools	Ramírez et al., 2016	https://deeptools.readthedocs.io/en/develop/
Image Studio version 5.2.5	LI-COR	http://opensource.licor.com/licenses/ImageStudio/index.html
MaxQuant version 1.5.2.8	Cox and Mann, 2008	https://www.maxquant.org/

RESOURCE AVAILABILITY**Lead contact**

Further information and requests for resources and reagents should be directed to the lead contact, Martin Eilers (martin.eilers@biozentrum.uni-wuerzburg.de).

Materials availability

Unique and stable reagents generated in this study are available upon request.

Data and code availability

The ChIP-Rx, BLISS and RNA sequencing data are deposited at the GEO (Gene Expression Omnibus) database (GEO accession: GSE150217). Original image data have been deposited to Mendeley Data: 10.17632/n4rr8ck4w3.1

EXPERIMENTAL MODEL AND SUBJECT DETAILS**Cell cultures, primary cells, viral strains**

HEK293TN, NIH 3T3 and U2OS cells were grown in DMEM (Sigma-Aldrich and Thermo Fisher Scientific). K562 were grown in RPMI 1640 supplemented with 4 mM Glutamine. Medium was supplemented with 10% fetal calf serum (Biochrom and Sigma-Aldrich) and penicillin–streptomycin (Sigma-Aldrich). All cells were routinely tested for mycoplasma contamination.

Cell line manipulation and generation

Lentiviral packaging plasmids psPAX2 (Addgene 12260) and pMD2.G (Addgene 12259) were used to generate stable cell lines. Lentivirus production was carried out in HEK293 cells and cell-free, virus-containing supernatant was used for infections. If not specified otherwise inhibitor treatment of U2OS cells was as follows: Doxycycline (24h, 1 μ g/ml), NVP-2 (3h, 1 μ M), LDC4297 (0.5 μ M, 3 h), BI8626 (10 μ M, 4h), NMS-873 (5 μ M, 4 h). BrdU (10 μ M) or EdU (10 μ M) treatment was for 30-60 min. Transfection with siRNA was performed using the RNAiMAX reagent (Thermo Fischer Scientific) according to the manufacturer's protocol. Cells were collected 40 h after transfection.

METHOD DETAILS**General cloning**

GST-MYC¹⁻¹⁶³ was cloned as described (Balupuri et al., 2019). GST-MYC¹⁻¹⁶³ Δ MBI and GST-MYC¹⁻¹⁶³ Δ MBII were cloned by PCR amplification using the primers MYC-f (pGex4T3) and MYC-r (pGex4T3) and inserted into pGex4T3 using EcoRI and XhoI restriction sites.

shRNA experiments

U2OS cells were infected with lentiviral supernatants in the presence of polybrene (4 μ g/ml) or protamine sulfate (5 μ g/ml) for 24 h. Medium (1:1, v/v) was added for 24 h. Cells were selected for 24 h with puromycin (2 μ g/ml) and afterward plated for the experiment. shRNAs against CTR9 and CDC73 were selected as described (Fellmann et al., 2013) and lentivirally transduced into the cell genome.

For Figures 1G, 2B, S1E, S1F, S1H, S1I, S2A, and S2B shRNA mirE3 against CDC73 was induced by doxycycline for 48 h. For Figures 1G, 2A, S1D, S1F, S1H, S1I, S2A, and S2B shRNA mirE3 against CTR9 was induced by doxycycline for 48 h. For Figures 1E, 1F, 6A–6D, S1A–S1C, S6A–S6C, and S6E shRNA mirE3 against CDC73 was constitutively expressed. For Figures 6A and 6B shRNA mirE4 against CDC73 was constitutively expressed. For Figures 1E, 1F, 5B, 6A–6E, 7A, S1A–S1C, S6A–S6E, and S7A shRNA mirE3 against CTR9 was constitutively expressed. For Figures 6A and 6B shRNA mirE5 against CTR9 was constitutively expressed.

Protein expression, purification, and in vitro pulldown

PAF1c (CTR9, Leo1, Paf1, CDC73, WDR61) was expressed and purified as described (Vos et al., 2018a). pGex4T3 plasmids (GST, GST-MYC¹⁻¹⁶³, GST-MYC¹⁻¹⁶³ΔMBI and GST-MYC¹⁻¹⁶³ΔMBII) were transformed into BL21 *E. coli* and preculture was incubated overnight. LB-media was inoculated until an OD600 of 0.5. Overexpression was induced with 100 mM IPTG for 6 h. Bacteria were pelleted and lysed in STE buffer (150 mM NaCl, 10 mM Tris/HCl pH 8, 1 mM EDTA, 0.5 mM TCEP, protease inhibitors (Sigma)). Lysate was sonicated for three times 1 min (1 s pulse on, 1 s pulse off) and centrifuged. Washed Sepharose beads (GE Healthcare/VWR International) were incubated with lysate for 1 h at 4°C. After coupling, beads were washed with STE buffer. GST and GST-MYC¹⁻¹⁶³ were of the same preparation as described in Baluapuri et al. (2019). For *in vitro* pull-down, GST or GST-MYC¹⁻¹⁶³ as well as GST-MYC¹⁻¹⁶³ΔMBI and GST-MYC¹⁻¹⁶³ΔMBII coupled beads were washed with pull-down buffer (100 mM NaCl, 20 mM Na-HEPES pH 7.5, 4% glycerol, 3 mM MgCl₂, 1 mM 1,4-Dithiothreitol, 300 ng/ml BSA) and incubated with PAF1c overnight at 4°C on a rotating wheel. After pull-down, beads were washed with pull-down buffer and NETN buffer (20 mM Tris pH 8, 100 mM NaCl, 1 mM EDTA, 0.5% NP-40). Pull-down was eluted from beads in 2x Laemmli sample buffer (20 mM Tris pH 6.8, 4% SDS, 0.02% bromophenol blue, 13.4% glycerol, 2 mM 1,4-Dithiothreitol) at 95°C for 5 min.

Immunoblot

Cells were lysed in RIPA lysis buffer (50 mM HEPES pH 7.9, 140 mM NaCl, 1 mM EDTA, 1% Triton X-100, 0.1% SDS, 0.1% sodium deoxycholate) containing protease and phosphatase inhibitors (Sigma-Aldrich) and incubated for 20 min at 4°C with rotation. The lysate was cleared by centrifugation and protein concentration was determined using the BCA assay. The cell lysate (same number of cells or amount of protein) was separated by BisTris-PAGE and transferred to PVDF membranes (Millipore). Membranes were blocked for 1 h and probed using antibodies against total RNAPII (Santa Cruz Biotechnology, sc-55492, sc-17798), pS2-Pol II (Abcam, ab24758), MYC (Abcam, ab32072), CTR9 (Bethyl Laboratories, A301-395), CDC73 (Bethyl Laboratories, A300-171A), PAF1 (Abcam, ab20662), Leo1 (Novus Biologicals, NB600-276), GST (GE Healthcare/Sigma-Aldrich, GE27-4577-01), Vinculin (Sigma, V9131), CDK2 (Cell Signaling Technology, sc-163), CHK1 (Santa Cruz Biotechnology, sc-7898), phospho-Chk1 (Cell Signaling, 2348), phospho-Histone H2A.X (Cell Signaling, 2577), phospho-KAP1 (phospho S824, Abcam, ab70369), KAP1 (Bethyl Laboratories, A300-274A), Histone H2B (Abcam, ab1790), Ubiquityl-Histone H2B (Cell Signaling Technology, 5546), HUWE1 (Abcam, ab70161), mono- and polyubiquitinated conjugates (FK2, Enzo Life Sciences, BML-PW8810-0100). For visualization the LAS3000 or LAS4000 Mini (Fuji) or Odyssey CLx Imaging System (LICOR Biosciences) were used. Quantification was performed using Image Studio (LI-COR Biosciences, version 5.2.5).

Immunoprecipitation

Cells were resuspended in lysis buffer (20 mM HEPES pH 7.9, 180 mM NaCl, 1.5 mM magnesium dichloride, 10% glycerol, 0.2% NP-40) supplemented with a cocktail of protease and phosphatase inhibitors (Sigma-Aldrich) and 10 mM N-Ethylmaleinimid. After brief sonication, samples were incubated on ice for 30 min with 10 U Benzonase and cleared by centrifugation. Dynabeads (20 μL of Protein A/G beads, Thermo Fisher Scientific) were pre-incubated, overnight at 4°C with rotation, in the presence of 5 g/l BSA and 3 μg antibody targeting mono- and polyubiquitinated conjugates (Enzo Life Sciences, BML-PW8810-0100). Co-immunoprecipitation was carried out in lysis buffer with an adjusted amount of lysate according to protein concentration and incubated for 12 h at 4°C. Elution of dynabeads was performed by heating in 1.5x Laemmli sample buffer (15 mM Tris pH 6.8, 3% SDS, 0.015% bromophenol blue, 10% glycerol, 1.5 mM 1,4-Dithiothreitol) for 5 min at 95°C. Samples were analyzed by immunoblotting.

Chromatin IP without or with reference exogenous genome spike-in (ChIP, ChIP-Rx)

For each ChIP or ChIP-Rx sequencing experiment, 5x10⁷ cells per immunoprecipitation condition were fixed with formaldehyde (final concentration, 1%) for 5–10 min at room temperature. Fixation was stopped by adding 125 mM glycine for 5 min. Cells were harvested in ice-cold PBS containing protease and phosphatase inhibitors (Sigma-Aldrich). All further used buffers also contained protease and phosphatase inhibitors. As exogenous control (spike-in), murine NIH 3T3 cells were added at a 1:10 cell ratio during cell lysis. Cell lysis was carried out for 20 min in lysis buffer I (5 mM PIPES pH 8.0, 85 mM KCl, 0.5% NP-40) and nuclei were collected by centrifugation at 1500 rpm for 20 min at 4°C. Crosslinked chromatin was prepared in lysis buffer II (10 mM Tris pH 7.5, 150 mM NaCl, 1 mM EDTA, 1% NP-40, 1% sodium deoxycholate, 0.1% SDS) and fragmented by sonication (total duration, 20 min with 10 s pulses and 45 s pausing) or by using the Covaris Focused Ultrasonicator M220 for 50 min per ml lysate. Fragment size of 150–300 bp was validated by agarose gel electrophoresis. Chromatin was centrifuged for 20 min at 14,000 rpm at 4°C before IP. For each IP reaction, 100 μL Dynabeads Protein A and Protein G (Thermo Fisher Scientific) were pre-incubated overnight with rotation in the presence of 5 mg/ml BSA and 15 μg antibody (total Pol II (Santa Cruz Biotechnology, sc-17798), pS2-Pol II (Abcam, ab24758), MYC (Abcam, ab32072), CTR9 (Bethyl Laboratories, A301-395), CDC73 (Bethyl Laboratories, A300-171A), Histone H2B (Abcam, ab1790),

Ubiquitinyl-Histone H2B (Cell Signaling Technology, 5546), NELFC (Cell Signaling Technology, 12265S). Chromatin was added to the beads, and IP was performed for at least 6 h at 4°C with rotation. Beads were washed three times each with washing buffer I (20 mM Tris pH 8.1, 150 mM NaCl, 2 mM EDTA, 1% Triton X-100, 0.1% SDS), washing buffer II (20 mM Tris pH 8.1, 500 mM NaCl, 2 mM EDTA, 1% Triton X-100, 0.1% SDS), washing buffer III (10 mM Tris pH 8.1, 250 mM LiCl, 1 mM EDTA, 1% NP-40, 1% sodium deoxycholate; including a 5 min incubation with rotation), and TE buffer (Thermo Fisher Scientific). Chromatin was eluted twice by incubating with 150 mL elution buffer (100 mM NaHCO₃, 1% SDS) for 15 min with rotation. Input samples and eluted samples were de-crosslinked overnight. Protein and RNA were digested with proteinase K and RNase A, respectively. DNA was isolated by phenol-chloroform extraction and ethanol precipitation and analyzed by qPCR using StepOnePlus Real-Time PCR System (Thermo Fisher Scientific) and SYBR Green Master Mix (Thermo Fisher Scientific) or sequencing on the Illumina Next-Seq500.

For ChIP or ChIP-Rx sequencing, DNA was quantified using the Quant-iT PicoGreen dsDNA assay (Thermo Fisher Scientific). DNA library preparation was done using the NEBNext ChIP-Seq Library Prep Master Mix Set for Illumina (New England Biolabs) or NEBNext Ultra II DNA Library Prep Kit (New England Biolabs) following manufacturer's instructions. Quality of the library was assessed on the Fragment Analyzer (Agilent) using the NGS Fragment High Sensitivity Analysis Kit (1–6,000 bp; Agilent). Finally, libraries were subjected to cluster generation and base calling for 75 cycles on Illumina NextSeq500 platform.

Proximity ligation assay

2500 U2OS cells expressing doxycycline-inducible MYC were seeded per well in a 384 well format (PerkinElmer) and allowed to settle overnight. Where indicated, cells were treated with doxycycline (1 μg/ml, 24 h) or equal amounts of ethanol. 4 h before fixation with 4% paraformaldehyde, the indicated inhibitors or equal amounts of DMSO were added if indicated. Fixed cells were permeabilized with 0.3% Triton X-100, washed in PBS, and blocked (5% BSA in PBS) for 60 min. Cells were incubated overnight at 4°C with primary antibodies against MYC (Santa Cruz Biotechnolog, sc-42), PAF1 (Abcam, ab20662), pS5-RNAPII (Biolegend, 904001) in 5% BSA in PBS. Cells were treated for 1 h at 37°C with plus (Sigma-Aldrich, DUO92002) and minus (Sigma-Aldrich, DUO92004) probes directed at rabbit and mouse antibodies, respectively, and ligated for 30 min at 37°C. Next, *in situ* PCR amplification was done with Alexa 488-conjugated oligonucleotides (Sigma-Aldrich, DUO92014) for 2 h at 37°C. Samples were counter-stained with Hoechst 33342 (Thermo Fisher Scientific). Image acquisition was done using the Operetta CLS High-Content Analysis System with 40x magnification (PerkinElmer) and were processed using Harmony High Content Imaging and Analysis Software (PerkinElmer) and R. Wells with focus error were discarded.

siRNA screen

1,250 U2OS cells expressing doxycycline-inducible MYC were seeded per well in a 384 well format (PerkinElmer) and allowed to settle for 10 h. Transfection was performed using RNAiMAX reagent (Thermo Fisher Scientific) according to manufacturer's protocol using a pool of 4 siRNAs against each listed E3-ligase from ubiquitin conjugation libraries (Dharmacon, GU-105635, GU-105625, GU-105615). 16 h post transfection 1 μg/ml doxycycline or equal amounts of ethanol were added for 24 h. Where indicated, MG132 (20 μM, Calbiochem / Merck) was added 4 h before fixation with 4% paraformaldehyde. Proximity Ligation Assay was performed as described. The readout parameter for statistical analysis was foci/nucleus as produced by the Harmony High Content Imaging and Analysis Software (PerkinElmer). Statistical analysis was performed in R by calculating the fold change to the non-targeting siRNA of the respective replicate and applying Welch's t test over all replicates for each siRNA to the non-targeting control with subsequent correction for multiple testing using Benjamini and Hochberg's *FDR* method. To reduce the influence of outliers, generated by transfection, Proximity Ligation Assay and image acquisition, a modified Z-score ("robust Z-score") (Iglewicz and Hoaglin, 1993) was calculated as follows:

$$Z_{\text{rob}} = \frac{|x_i - \text{med}(x_{i,n})|}{1.4826 * \text{med}(|x_i - \text{med}(x_{i,n})|)}$$

BLISS8

The original BLISS protocol was adapted and modified from Yan et al. (2017). For experiments in U2OS cells expressing doxycycline inducible MYC, cells were plated in a 24-well plate (Greiner) and incubated with ethanol or doxycycline (1 μg/ml) from the following day onward for 24 h. Where indicated, etoposide was added (3 h, 25 μM). For Figure 5B U2OS cells expressing doxycycline-inducible MYC were infected with lentiviral supernatants in the presence of 4 μg/ml polybrene or protamine sulfate (5 μg/ml) for 24 h. Medium (1:1, v/v) was added for 24 h. Cells were selected for 24 h with puromycin (2 μg/ml) and afterward 20,000 control cells and 30,000 cells expressing a constitutive active shCTR9 were plated for the experiment. Cells were incubated with ethanol or doxycycline (1 μg/ml) for 24 h. Cells were fixed by addition of paraformaldehyde directly to the media to a final concentration of 3.7%, washed with PBS and either stored at 4°C or directly processed. For experiments in K562-AID cells, cells were transferred to 24-well plate 12 h before fixation and spun down 5 min preceding and during fixation. Lysis was performed by incubation in lysis buffer 1 (10 mM Tris-HCl, 10 mM NaCl, 1 mM EDTA, 0.2% Triton X-100, pH 8) for 1 h at 4°C, brief rinsing in PBS and incubation in lysis buffer 2 (10 mM Tris-HCl, 150 mM NaCl, 1 mM EDTA, 0.3% SDS, pH 8) for 1 h at 37°C. Following rinsing in PBS, cells were equilibrated in CutSmart buffer (New England Biolabs) previous to restriction enzyme digestion using AsiSi (New England Biolabs) according to manufacturer's protocol. Following rinsing in PBS and equilibrating the cells in CutSmart buffer, blunting of double-strand breaks using Quick

Blunting Kit (New England Biolabs) following manufacturer's protocol was performed. Sense and antisense adaptor-oligos were annealed by heating them for 5 min at 95°C, followed by a gradual cooldown to 25°C over a period of 45 min. Consecutive to equilibration in CutSmart buffer (New England Biolabs) and T4 Ligase buffer (New England Biolabs) annealed adapters were dispensed on samples and ligated using T4 DNA Ligase (New England Biolabs) using manufacturer's recommendations for 16 h at 16°C. Excessive Adapters were removed by repeated rinsing in a high-salt wash buffer (10 mM Tris-HCl, 2M NaCl, 2 mM EDTA, 0.5% Triton X-100, pH 8). Genomic DNA was extracted in DNA extraction buffer (1% SDS, 100 mM NaCl, 50 mM EDTA, 10 mM Tris-HCl, pH 8) supplemented with Proteinase K (1 mg/ml, Roth) for 16 h in a thermo-shaker at 55°C. DNA was isolated by phenol-chloroform extraction and isopropanol precipitation, resuspended in TE buffer and sonicated using the Covaris Focused Ultrasonicator M220 for 1 to 2 min to achieve a fragment size of 300-500 bp. Fragment size was assessed on the Fragment Analyzer (Agilent) using the NGS Fragment High Sensitivity Analysis Kit (1-6,000 bp; Agilent). The DNA was concentrated using Agentcourt AMPure XP Beads (Beckman Coulter), transcribed into RNA and DNA digested using MEGAscript T7 Transcription Kit (Thermo Fischer Scientific) following manufacturer's recommendations. A two-sided RNA cleanup with a ratio of 0.4 followed by 0.2x was performed using Agentcourt RNAClean XP Beads (Beckman Coulter). RNA concentration was assessed on the Fragment Analyzer (Agilent) by using Standard Sensitivity RNA Analysis Kit (Agilent). Library preparation was performed by ligating the RA3 adaptor to the samples with a T4 RNA Ligase 2 (New England Biolabs) supplemented with Recombinant Ribonuclease Inhibitor (Thermo Fischer Scientific). Samples were reverse transcribed using SuperScript III Reverse Transcriptase kit (Thermo Fischer Scientific) and library indexing and amplification performed using NEBNext High-Fidelity 2X PCR Master Mix (New England Biolabs) with RP1- and desired RPI-primer with 18 (Figure 5A), 19 cycles (Figure 5B) or 17 cycles (Figure S5C) with half of the amount of the prepared library. The libraries were cleaned up using Agentcourt AMPure XP Beads (Beckman Coulter), quality, quantity, and fragment size assessed on the Fragment Analyzer (Agilent) using the NGS Fragment High Sensitivity Analysis Kit (1-6,000 bp; Agilent) and subsequently subjected to Illumina NextSeq 500 sequencing, according to manufacturer's instructions. Adapters and oligos were custom synthesized and Unique Molecular Identifiers (UMIs) generated by random incorporation of the four standard dNTPs using the 'Machine mixing' option.

Cell Cycle Immunofluorescence

For Figure 5D U2OS cells expressing doxycycline inducible MYC were plated in a 96-well plate (Greiner) and incubated with ethanol or doxycycline (1 µg/ml) from the following day onward for 24 h. Where indicated, etoposide was added (3 h, 25 µM, Sigma-Aldrich). For Figures 6E and S6D U2OS cells expressing doxycycline inducible MYC were infected with lentiviral supernatants in the presence of 4 µg/ml polybrene or protamine sulfate (5 µg/ml) for 24 h. Medium (1:1, v/v) was added for 24 h. Cells were selected for 24 h with puromycin (2 µg/ml) and afterward plated for the experiment. Cells were pulsed with 10 µM EdU (Jena Bioscience) for 30 min and subsequently fixed with 3.7% paraformaldehyde in PBS. After removing paraformaldehyde and washing with PBS, cells were permeabilized with 0.3% Triton X-100 in PBS and blocked with 5% BSA in PBS. Newly synthesized DNA was visualized by performing a copper(I)-catalyzed azide-alkyne cycloaddition (100 mM Tris pH 8.5, 4mM CuSO₄, 10mM AFDye 647 Azide (Jena Bioscience), 10mM L-Ascorbic Acid). Samples were stained with primary antibodies against phospho-Histone H2A.X (Cell Signaling, 2577) in 5% BSA in PBS overnight at 4°C and after rinsing with PBS, incubated with secondary antibody (Thermo Fisher Scientific, A-11029) for 1 h at room temperature. Counter-staining was performed using Hoechst 33342 (Sigma-Aldrich). Images were taken with an Operetta High-Content Imaging System with 20x magnification. Images were processed using Harmony High Content Imaging and Analysis Software and R. Cells were grouped into cell cycle phase according to EdU and Hoechst staining of the control condition.

Confocal microscopy

Leica SP8 (DM6000) upright microscope was used to scan all cells under 63x GLY objective with HyD detector for EdU channel and PMT for γ-H2AX at 400 Hz scan rate. Stacks with planes 330 nm apart were taken under same gain and laser power values for all conditions.

Image processing and colocalization quantification

3-5 planes of each stack were converted to a single image via maximum intensity projection followed by addition of a Gaussian blur filter with sigma value of 0.8. Composite images of all channels were created, and representative line profiles were generated using "Plot Profile" function in ImageJ over a width of single Gaussian corrected pixel. Pearson's correlation constant was calculated for brightness and contrast corrected images (EdU – min. values 10–20 and max. values 90–150; pgH2AX – min. values 10 and max. values 90–125) using Coloc 2 plugin in ImageJ (https://imagej.net/Coloc_2).

RNA sequencing

U2OS cells expressing doxycycline inducible MYC were infected with lentiviral supernatants in the presence of 4 µg/ml polybrene or protamine sulfate (5 µg/ml) for 24 h. Medium (1:1, v/v) was added for 24 h. Cells were selected for 24 h with puromycin (2 µg/ml) and afterward plated for the experiment. Cells were incubated with ethanol or doxycycline (1 µg/ml) for 24 h. Treatment was stopped by adding RLT Buffer (QIAGEN) containing β-Mercaptoethanol according to instruction manual. Total RNA was extracted using RNeasy mini column (QIAGEN) including on-column DNase I digestion. mRNA was isolated using NEBNext Poly(A) mRNA Magnetic Isolation Module (NEB) and library preparation was performed with the NEBNext Ultra RNA Library Prep Kit for Illumina following the instruction manual. Libraries were size selected using Agentcourt AMPure XP Beads (Beckman Coulter), followed by amplification

with 12 PCR cycles. RNA quality was assessed on the Fragment Analyzer (Agilent) by using Standard Sensitivity RNA Analysis Kit (Agilent).

Flow cytometry

U2OS cells expressing doxycycline inducible MYC were infected with lentiviral supernatants in the presence of 4 $\mu\text{g/ml}$ polybrene or protamine sulfate (5 $\mu\text{g/ml}$) for 24 h. Medium (1:1, v/v) was added for 24 h. Cells were selected for 24 h with puromycin (2 $\mu\text{g/ml}$) and afterward plated on a 6 cm dish. Cells were labeled with 10 μM 5-Bromo-2'-deoxyuridine (BrdU, Sigma) for 30- 50 min. Both supernatant and cells were harvested. Cell pellets were washed with ice-cold PBS and fixed with ice-cold 80% ethanol, then incubated at -20°C overnight. The cells were collected by centrifugation, washed with ice-cold PBS and incubated in 2 M HCl with 0.5% Triton X-100 for 30 min at room temperature. Cell pellets were neutralized with Natriumtetraborat. Anti-BrdU-FITC antibody (BD Biosciences, BLD-364104) incubation was done in 100 μL 1% BSA-PBS-T (0.5% Tween-20 in PBS) for 30 min at room temperature in the dark. Then cells were washed with 1% BSA-PBS-T and incubated in PBS and 24 $\mu\text{g/ml}$ RNase A (Roche) at 4°C over night in the dark. Data were acquired using the FACScanto II (BD Biosciences).

Colony formation assay

U2OS cells expressing doxycycline inducible MYC were infected with lentiviral supernatants in the presence of 4 $\mu\text{g/ml}$ polybrene or protamine sulfate (5 $\mu\text{g/ml}$) for 24 h. Medium (1:1, v/v) was added for 24 h. Cells were selected for 24 h with puromycin (2 $\mu\text{g/ml}$) and afterward plated on a 6-well plate. Cells were incubated with ethanol or doxycycline (1 $\mu\text{g/ml}$) for 24 h. Cells were fixed with 70% ethanol, dried, and stained with crystal violet.

Knockin of the HUWE1 catalytic mutant in HCT116 cells

The HUWE1 repair template included the sequence of human HUWE1 ORF (ENST00000342160.7) that encodes protein residues 4277-4374 of the isoform Q7Z6Z7-1 (with either cysteine or serine at position 4341), the P2A self-cleaving peptide, a blasticidin resistance gene, and homology arms spanning genomic positions chrX:53561159-53561889 and chrX:53559367-53560269. Two sgRNAs against HUWE1 were cloned in the PX459 vector (kind gift from Feng Zhang, Addgene 62988) and co-transfected with the repair template plasmid in the HCT116 cells using the Fugene reagent (Promega). Transfected cells were selected with puromycin and blasticidin (InvivoGen). Individual clones were validated by PCR and Sanger sequencing of genomic DNA and mRNA.

SILAC-based ubiquitin remnant profiling

U2OS SILAC-labeled cells were transfected with siRNAs targeting non-targeting control or HUWE1 as previously described or treated with BI8626 (10 μM , 24 h). Cells were lysed in modified RIPA buffer (50 mM Tris pH 7.5, 150 mM NaCl, 1 mM EDTA, 1% NP-40, 0.1% sodium deoxycholate) supplemented with protease inhibitors (Complete protease inhibitor cocktail tablets, Roche Diagnostics), 1 mM sodium orthovanadate, 5 mM β -glycerophosphate, 5 mM sodium fluoride and 10 mM N-ethylmaleimide. Proteins were digested with endoproteinase Lys-C (Wako Chemicals) and sequencing grade modified trypsin (Sigma-Aldrich). Modified peptide enrichment was done using di-glycine-lysine antibody resin (Cell Signaling Technology, 5562). Peptides were analyzed on a quadrupole Orbitrap mass spectrometer (Q Exactive Plus, Thermo Scientific) equipped with a UHPLC system (EASY-nLC 1000, Thermo Scientific) as described (Kelstrup et al., 2012; Michalski et al., 2012). MaxQuant (development version 1.5.2.8) was used to analyze the raw data files (Cox and Mann, 2008). Parent ion and MS² spectra were searched against a human protein database obtained from UniProtKB released in May 2016 using Andromeda search engine (Cox et al., 2011). Experimental details were described previously (Heidelberg et al., 2018).

Bioinformatics

Sequencing libraries were subjected to Illumina NextSeq 500 sequencing according to the manufacturer's instructions. After base calling with Illumina's FASTQ Generation software v1.0.0 (NextSeq 500 sequencing), high quality PF-clusters were selected for further analyses and sequencing quality was ascertained using FastQC. ChIP samples were mapped to human hg19 and ChIP-Rx samples were mapped separately to the human hg19 and to the murine mm10 genome using Bowtie1 (Langmead et al., 2009) or Bowtie 2 (Langmead and Salzberg, 2012) with default parameters. ChIP samples were normalized to the number of mapped reads in the smallest sample. For ChIP-Rx spike-in normalized reads were calculated by dividing the number of mapped reads mapped to hg19 by the number of reads mapped to mm10 for each sample and multiplying this ratio with the smallest number of reads mapped to mm10 for any sample. RNaseq samples were mapped to hg19 using Bowtie2 (Langmead and Salzberg, 2012) and samples were normalized to the number of mapped reads in the smallest sample. Reads per gene were counted using the "summarizeOverlaps" function from the R package "GenomicAlignments" using the "union"-mode and Ensembl genes. Non- and weakly expressed genes were removed (mean count over all samples < 1). Differentially expressed genes were called with edgeR and p values were adjusted for multiple-testing using the Benjamini-Höchberg procedure. Metagene plots were generated with ngs.plot.r (Shen et al., 2014). Non-scaled density plots were produced with the plotProfile program from the DeepTools suite (Ramírez et al., 2016). Bin plots (Figure 6B) were drawn using R, by ordering 13'337 genes with significant expression in U2OS cells according to their inducibility by over-expressed MYC (Walz et al., 2014) into bins of 600 genes each. For each bin, the average expression ratio in control cells ("EtOH) or cells overexpressing MYC ("Dox) in the presence of the indicated shRNA was plotted on the Y axis, against the average inducibility by

overexpressed MYC as derived from Walz et al. (2014) on the X axis (ratio “Dox / EtOH”). MYC-reads in promoter or enhancer regions were determined by processing read-normalized MYC ChIPseq bam-files with the BEDtools intersectBed program (Quinlan and Hall, 2010). Promoter regions were defined here as TSS \pm 1 kb, and enhancer regions were as previously defined (Walz et al., 2014). MYC-activated and -repressed genes were derived from Lorenzin et al. (2016).

BLISS8 samples were demultiplexed based on their condition-specific barcodes using UMI-tools (Smith et al., 2017), allowing 1 mismatch in the barcode, and separately mapped to hg19 using Bowtie2 (Langmead and Salzberg, 2012) with default parameters. For Figures 5A, 5B, and S5C, respective samples of biological triplicates were merged preceding to mapping and collectively processed. Samples were filtered against an ENCODE Blacklist file to remove regions of high variance in mappability commonly found in satellite, centromeric and telomeric repeats (Amemiya et al., 2019) using bedtools intersect (Quinlan and Hall, 2010). To allow absolute quantification of double-strand breaks and remove PCR-introduced artifacts, duplicated reads were identified based on their UMI, grouped and deduplicated using UMI-tools (Smith et al., 2017) with default parameters. For normalization, deduplicated reads in AsiSI specific restriction sites were counted using countBamInGRanges from the R package exomeCopy. The sample with the smallest number of AsiSI specific reads was divided by the number of respective reads from each sample. Resulting ratio was multiplied by the total amount of deduplicated reads and samples subsequently randomly subsampled to the calculated number of reads. AsiSI specific restriction sites were generated by *in silico* digestion of the hg19 genome. From the 1,123 predicted restriction sites, sites without mapped reads across all conditions in the respective experiment were dropped. BLISS8 density profiles were generated using the R package *metagene2* with the assay parameter ‘ChIPseq’, 150 bp read extension and 50 bins to smoothen the graph. Promoter counts were generated using the R package *exomeCopy* in the region of 500 bp up- and downstream of the annotated transcriptional start site and divided by the number of genes in the corresponding gene set. Gene sets were generated from RNA sequencing data using RPKM (gene expression) and logCPM (MYC response), or RNAPII ChIP-Rx data using the occupancy in the gene body versus the occupancy in the corresponding promoter region (pausing). Heterochromatic regions in U2OS were identified using a 16-state model (Ho et al., 2014) with chromHMM (Ernst and Kellis, 2012) and published datasets for H3K9me3 (Tasselli et al., 2016), H3K4me3, H3K27me3 (Easwaran et al., 2012), H3K79me2 (Clouaire et al., 2018), H3K36me3 (Wen et al., 2014), H3K4me1, H3K27ac (Walz et al., 2014).

Subsets of genes were derived from our RNaseq data in U2OS as well as from published U2OS ChIPseq data (Lorenzin et al., 2016; 3000 most/least expressed genes passing the minimal expression threshold; MYC-bound: 7684 genes that are expressed in U2OS according to our RNaseq data and contain a MYC-binding site in the region between –1500 and +500 relative to the transcription start site; non MYC-bound: 10013 expressed genes lacking such a MYC binding site; the former group was further subdivided based on the presence of a canonical E-box sequence [CACGTG] within 100 nucleotides of their MYC-binding summit, producing subgroups of 1169 and 6515 genes, respectively). BLISS8 stratification by expression is based on published K562 polyA-RNaseq data from the ENCODE portal (<https://www.encodeproject.org/>) with the following identifiers: ENCSR040YBR. The R dataset *TxDb.Hsapiens.UCSC.hg19.knownGene* was subsampled using the selected 5,576 bottom and 5,458 top expressed genes and filtered for a minimum gene length of 1500 bp. Further stratifications are based on respective lists mentioned in this paragraph and adapted as described. Artifacts produced by proximal downstream transcriptional start sites were filtered out. For Figure 5C the number of double strand breaks is presented relative to the number of genes per group, stratified by expression (top $n = 3,177$, bottom $n = 1,814$), pausing of RNAPII (paused $n = 3414$, non-paused $n = 671$), and response to MYC (activated $n = 340$, repressed $n = 296$).

QUANTIFICATION AND STATISTICAL ANALYSIS

General statistics

Statistical significance in Figures 3A and S3A was determined by applying Wilcoxon rank sum test. Statistical analysis in Figures 3B and S3B was performed in R by calculating the fold change to the non-targeting siRNA of the respective replicate and applying Welch’s t test over all replicates for each siRNA to the non-targeting control with subsequent correction for multiple testing using Benjamini and Hochberg’s FDR method. For Figures 4F and S5E, statistical significance was determined by applying the Welch’s t test. For Figure 5C significance was calculated applying Wilcoxon rank sum test. Correlation and respective p value were calculated using the Pearson product-moment correlation coefficient for the shown experiment in Figure S3C (left). Statistical significance in Figure S3C (right) was calculated using the R package *limma* across all biological replicates and corrected for multiple testing using Benjamini and Hochberg’s FDR method. For Figures 6E and S6E Wilcoxon test was used to calculate the significance. To calculate the significance in Figure S6E the different conditions were compared against the reference group (“shNTC EtOH”) within one cell cycle phase. For Figures S1A and S1I the relevant samples were compared using a unpaired t test.